Acknowledgments

We would like to thank our supervisor, Dr. Alberto Aliseda, for his comments always right, and his support during our project.

We would also thank our tutor, Teymour Javaherchi, for his availability, patience and kindness during and after work. We address our thanks to Samantha Adamski, for her support in our many computer issues.

Lastly, we would offer our regards to CC. François Nevejans, for his trust in our project.

NUMERICAL STUDY OF HORIZONTAL AXIS HYDROKINETIC TURBINES: PERFORMANCE ANALYSIS AND ARRAY OPTIMIZATION

PFE n°: GM01

Students: Ensigns M. **TESSIER** and N. **TOMASINI**, EN 2010

Departments: Maritime Engineering Department

Host institution of studies: **Department of mechanical engineering, University of Washington – Seattle (WA), USA**

Director of research: Associate Professor, A. Aliseda

Tutor of project: PHD Student T. Javaherchi

Corresponding officer: CC F. NEVEJANS

ABSTRACT

Horizontal Axis Hydrokinetic Turbine is a novel, predictable, renewable energy, but to implement it at a large scale, significant research have to be conducted. Considering the cost of experimental studies, a cheaper method has been chosen, computational fluid dynamics. A new shape of blade is studied, the DOE reference model 1. A study as a single turbine and as an array of turbine is performed. To reduce the computational time and also to be the more accurate, several computational and physical parameters have to be determined. For a single turbine, the correlation between two computational models is studied. Then, an analysis of the extracted power is possible. Once the single turbine is well characterized, it is possible to perform an array optimization. All this work is based on previous research on array optimization done at the University of Washington laboratory and also on the singe turbine work done in the first part of this project.

RESUME

Les turbines hydro cinétiques à axe horizontal sont une nouvelle source d'énergie renouvelable très prévisible. Mais pour pouvoir les mettre en place à grande échelle, d'importantes recherches doivent être menés. Une étude expérimentale se révèle être très chère, une méthode moins couteuse est donc choisie, la modélisation informatique (CFD). Un nouveau prototype de pale est étudié, le DOE reference model 1. Une étude sur une seule turbine et ensuite sur un réseau de plusieurs turbines est menée. Mais pour réduire les temps de calculs et être le plus précis possible, plusieurs paramètres physiques et informatiques doivent être déterminés. Pour une seule turbine, la corrélation entre deux modèles de calcul est faite. Ensuite, une analyse des puissances extraites est rendue possible. Une fois la turbine bien définie, il est possible de procéder à l'optimisation d'un réseau de plusieurs turbines. Cette étude est réalisée à partir des précédents travaux effectues au laboratoire de l'*University of Washington* ,mais également grâce à l'étude d'une seule turbine réalisée dans la première partie de ce projet.

Key words: Renewable energy, Tidal turbine, Numerical model

Table of Contents

INTRODUCTION

Global warming and exhaustion of fossil energies are becoming serious issues in the early 21st century. Because of the need for new energy sources, renewable energy has emerged and is increasing its contribution to worldwide energy supply. Following the same concepts used in wind turbines, it has been decided to extract power from another natural element, the ocean. Tidal currents present an advantage compared to wind, it is predictable. Considering this, it is possible to calculate the amount of electricity that an array of tidal turbine could produce over a year. As the density of water is a thousand times higher than the density of air, the power density that can be extracted from a single location is also higher.

The purpose of the studies that are being carried out all around the world by different laboratories and companies is to successfully develop maritime hydrokinetic energy conversion with the highest efficiency possible. Several prototypes of turbines exist, and before building and testing them, numerical modeling can be used in order to predict the different phenomena that are going to occur around those turbines, as accurately as possible. It should also be noticed that these studies could be used to evaluate some possible environmental effects (for example sedimentation).

Numerical modeling is an inexpensive solution (in both time and cost) compared to experimental research to carry out preliminary studies that predict the behavior of the turbine and of the flow around the rotor. But to obtain results that accurately model reality, many parameters have to be set correctly. The estimated performance of the turbine will change as a function of those settings. The final goal is to accurately predict the performance of an array of turbines. But to be able to do this study, a single turbine must first be well characterized.

The goal of this project is to perform a numerical study of a horizontal axis hydrokinetic turbine, to analyze the performance of a single turbine and then to evaluate the performance of an optimized array.
After presenting the context of the study and the different theoretical and numerical tools, these elements will be used to analyze and validate two numerical models and the corresponding parameters for a single turbine. In a second part of the project, we will be able to perform an analysis of an array of turbines based on previous work done by the laboratory ([1], [2], [3], [4] and [5]).

I) CONTEXT OF THE STUDY

I.1) Why tidal energy?

Earth's surface is covered with approximately 75% of water. Gravitational attraction force of the moon is responsible for an observed phenomenon on the ocean called tidal movement. Depending on the geographical place and the type of cost, the type of tides appears in very different ways. For example in Western Europe semi diurnal tides is mostly prevalent meanwhile on the Pacific coast of the United States it is the mixed tides [4].
Knowing the characteristic of the tide in a channel is important, particularly the velocity and the direction. The kinetic energy flux in a tidal current channel is resulting from the velocity of water through a cross section. It is expressed by the following equation:

$$P = \frac{1}{2}\rho S \overline{V}^3 \quad (1)$$

Where ρ is the density of water, S is the surface of that section; and V is the average water velocity perpendicular to the channel, that is obtained by integrating the local velocities perpendicular to the channel V on the surface S:

$$\overline{V} = \int V dS \quad (2)$$

The prevalent term in equation (1) is the velocity one because it is cubed, so the velocity mostly influences the kinetic energy flux, and is directly the power extracted from a tidal turbine. That is why every place on the world does not suit well for the implantation of tidal turbines and that a site with tidal current speeds exceeding 2 $m.s^{-1}$ has a high renewable energy potential.
The state of Washington and more particularly the area of Seattle have a high renewable energy potential. In the Strait of Juan de Fuca the current velocity is in average 2 $m.s^{-1}$. (Figure 1). This is why there is a real potential and why the University of Washington is doing research on this new technology.

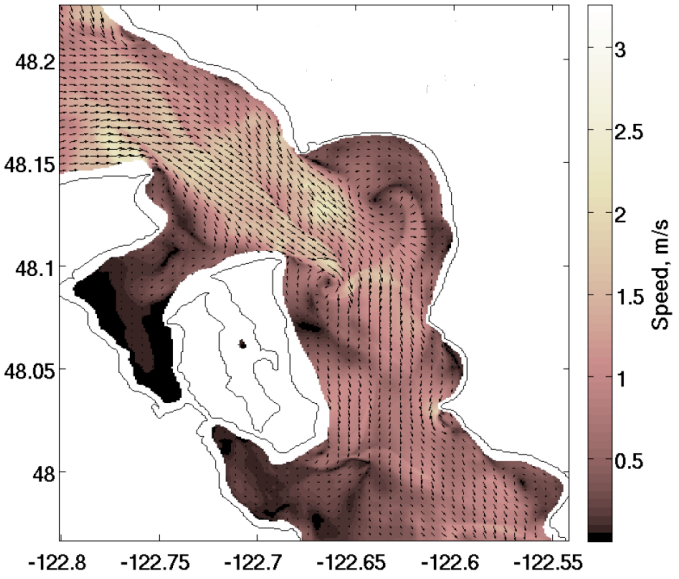

Figure n°1: Snapshot of speed at peak flood [6]

On another hand, due to shipping and navigation in this area, the space available with enough depth is restricted. Because the turbine studied is a 20 meters diameter one, a depth of 40 meters minimum is needed, in order to get rid of most of the interactions with the sea floor and to allow navigation in this area (Figure 2).

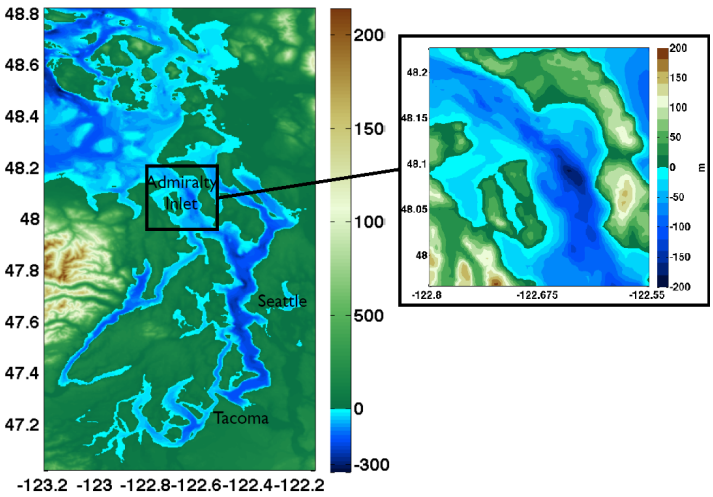

Figure n°2: Pudget Sound [6]

I-2) Motivation and Goals

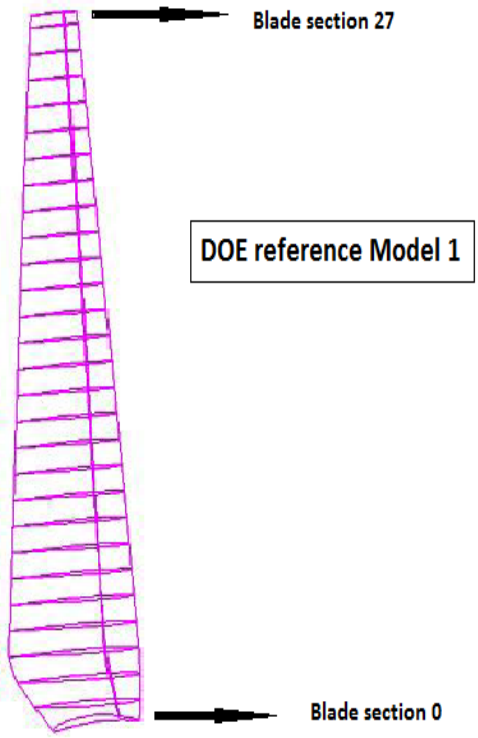

An economical application of Marine Hydrokinetic turbines (MHK) in a large scale is not realized. Industry and laboratory are still searching for the best way to extract tidal power from the ocean. Many models of tidal current energy converters are developed all around the world. But in reality we can distinguish four different concepts: Venturi Systems, Variable Foil Systems, Vertical Axis Turbine and the one which interest us, the Horizontal Axis Tidal Turbines (HATT) [4].

The choice of the HATTs has been motivated by the existence and the good knowledge of Horizontal Axis Wind Turbine. In this way a comparison was always possible to valid or not the results. The main difference between the two studies is the characteristics of the flows in interaction with the technology (Slightly higher Reynolds number and typical lower Tip Speed Ratios).

Figure n°3: DOE reference Model 1 – Blade sections

The methodology to study HATT has been validated with the help of the results provided by the National Renewable Energy Laboratory (NREL) who has published freely the results of his simulations on the NREL phase VI model.
Now that the methodology is well known and validated, thanks to the previous research, NREL has developed and designed a two bladed Horizontal Axis Hydrokinetic Turbine (HAHT). The official name of this prototype is DOE Reference Model 1 (Figure 3*)*, where DOE stands for Department of Energy, an entity which includes the NREL. In the Northwest National Marine Renewable Energy Center (NNMREC), University of Washington, a scaled prototype has been realized and is tested in a water tunnel near Vancouver (Canada) during our internship (Figure 4*)*. A comparison between the results provided by our study and the value provided by the test of the prototype could be the subject of further researches.
The basis of our study is essentially Mr. CERISOLA Arthur work [5] on the Single Rotating reference Frame (SRF) of the DOE Reference Model 1 and the optimization of an array of turbine. All the methodology developed by the Fluid Mechanics Lab of the Engineering Department of the University of Washington (Seattle, USA) will be applied.

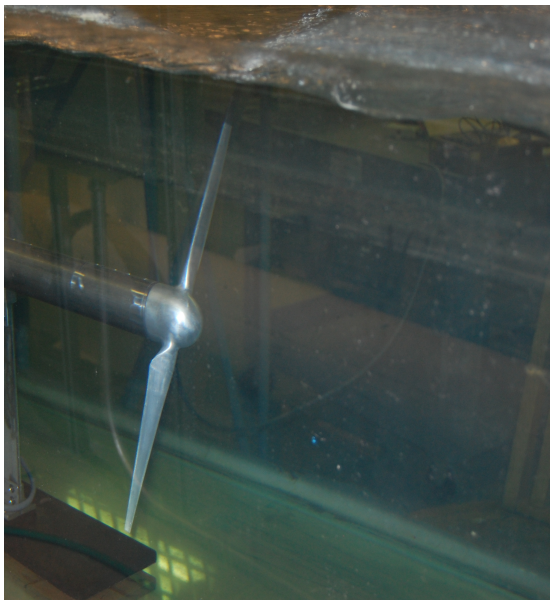

Figure n°4: Experimental test

I-3) Methodology

The methodology for this entire project is the one the laboratory has developed since several years. All the different methods will be describe more precisely further in the report. First a SRF mesh of the blade we are studying has been realized on the software GAMBIT. Then, using the software FLUENT, you can extract the X, Y, Z forces and the centers of pressure after running a simulation. Knowing the geometry, the characteristics of the blade, and the local velocity around the blade for the operating conditions, the lift and drag coefficients and the corresponding angles of attack can be calculated.
Then, a table giving the lift and drag coefficient in function of the angle of attack is built in order to use it in the Virtual Blade Model (VBM). A mesh of the VBM has to be created to launch simulations on FLUENT with the user's defined function corresponding to VBM. After adjusting the parameters on the VBM to match the SRF simulations, you can use it as a reference, and have the advantage to run simulations slightly faster.
To take into account the hub - to define more precisely the wake of the turbine - you model it with the Actuator Disk Model theory (ADM) that is add to the VBM.
After validating the VBM+ADM by matching results with the SRF, it is possible to work on different configurations of arrays of turbines. It is know possible to extract data as the power generated by the configuration of the array. The configurations studied here are the optimized ones found in previous report.

II) PHYSICAL AND NUMERICAL MODELS

II.1) Physical notions

This section was written based on references [3] and [7].

II.1.1) Navier-Stokes equation

The Navier-Stokes equations describe the motion of a fluid, using the Newton's second law of dynamics.
The fluid considered in this study is a Newtonian fluid, which respects the following assumptions: the fluid density ρ is constant, the fluid dynamic viscosity μ is constant, and the fluid is incompressible.
The general form of Navier-Stokes equation is the following:

$$\rho\frac{\partial\vec{u}}{\partial t} + \rho\vec{u}.\nabla\vec{u} = \mu\nabla^2\vec{u} - \nabla p + \vec{F} \quad (3)$$

where u is the velocity of the fluid and p is the pressure.
The physical meaning of different terms is described here:

- $\rho\frac{\partial\vec{u}}{\partial t}$: unsteady acceleration
- $\rho\vec{u}.\nabla\vec{u}$: convective acceleration
- ∇p: pressure gradient
- $\mu\nabla^2\vec{u}$: viscous forces
- $\vec{F}$: external forces such as gravity or centrifugal forces.

In order to simplify this equation, to be able to solve it with computational fluid model (CFD), the behavior of the fluid (laminar or turbulent) has to be characterized, using the Reynolds number defined as follows:

$$\mathrm{Re} = \frac{\rho U_\infty D}{\mu} \quad (4)$$

This number represents the ratio of inertial forces to viscous forces. A low Reynolds number means that viscous forces are dominant over inertial forces, and that the fluid is laminar. A high Reynolds number (i.e. larger than 5.10^5) means the fluid is turbulent. Inertial forces are dominant over viscous forces.
The fluid studied here is water liquid (with a density ρ either equal to 998.2kg.m^{-3} for water, or 1025kg.m^{-3} for seawater) and has a Reynolds number order of 10^7. It is turbulent.

II.1.2) RANS equations

Computers are not able to solve the Navier-Stokes equation because of the high fluctuations of turbulent flows. Indeed, they don't solve themselves equations but take algorithm written by engineers. When we take into account the turbulent fluctuations, the reformatted Navier-Stokes equations will have more unknown than the number of equations. Therefore, we will need a closure model to close the system of equations (i.e. having the same numbers of unknown and equations). The approach to define the fluctuations is the Reynolds decomposition. The flow variables are separated into the averaged component and the fluctuation component as described here for the velocity u and the pressure p:

$$u = \overline{u} + u' \tag{5}$$

$$p = \overline{p} + p' \tag{6}$$

The Navier-Stokes equation can be rewritten with the tensor notation as following:

$$\rho\frac{\partial u_i}{\partial t} + \rho\frac{\partial u_i u_j}{\partial x_j} = \mu\frac{\partial^2 u_i}{\partial x_i \partial x_j} - \frac{\partial p}{\partial x_i} + f_i \tag{7}$$

By substituting equations (5) and (6) in equation (7), the Reynolds Averged Navier-Stokes equation for the conservation of the momentum is obtained.

$$\rho\frac{\partial \overline{u}_i}{\partial t} + \rho\frac{\partial \overline{u}_i \overline{u}_j}{\partial x_j} = \frac{\partial}{\partial x_j}(\mu(\frac{\partial \overline{u}_i}{\partial x_j} + \frac{\partial \overline{u}_j}{\partial x_i})) - \frac{\partial \overline{p}}{\partial x_i} + f_i - \rho\frac{\partial \overline{u}_i' \overline{u}_j'}{\partial x_j} \tag{8}$$

Two new terms appear compared to the Navier-Stokes equation: the Reynolds Stress number $\rho\overline{u}_i'\overline{u}_j'$; and the mean rate of Strain tensor $S_{i,j} = \frac{1}{2}(\frac{\partial \overline{u}_i}{\partial x_j} + \frac{\partial \overline{u}_j}{\partial x_i})$.

These terms can be interpreted as components of a stress tensor, and increase laminar stresses due to the fluctuation. As a consequence, to describe a turbulent flow, we need to determine the two last terms: for that, we use a turbulence model.

II.1.3) Turbulence models

In this study, two different turbulence models were used: Spalart Allmaras, which is based on one transport equation added to the RANS equations, and the SST k-ω (shear stress transport k-ω) model based on two transport equations. The Spalart Allmaras model solves the transport equation for the turbulent viscosity ν_t . The SST k-ω is a modified model of the k-ω model, which uses the k-ω model near the blade and the k-ε model in the wake of the flow. k represents the turbulent kinetic energy, ω the turbulent frequency and ε the dissipation rate of turbulent kinetic energy. The last turbulence model uses these variables to solve the transport equations [8].
The two turbulence models applied for the study uses constant numbers that are based on empirical relations.

II.2) Numerical models

II.2.1) Single Rotating Reference Frame (SRF)

The Single Rotating Reference Frame (SRF) is the most expensive in computation time numerical model but it is also the one used as a reference for all the study. The SRF calculates the X,Y,Z forces on the blade, and also the center of pressure. With these values it is possible to obtain the lift and drag coefficient function of the angle of attack and then to run Virtual Blade Model simulations, which is less time consuming.

The base of the SRF is that it is not the blade that is rotating in the fluid but the fluid is rotating around the blade. The reference frame is changed. Consequently to this change fluid flow equations are no more solved in a stationary reference frame, which would be a transient problem, but in a rotating reference frame with the angular velocity of the turbine, which makes the problem steady state (figure 5). This change allows solving the equations easily even if two acceleration terms appear: Coriolis and Centripetal acceleration.

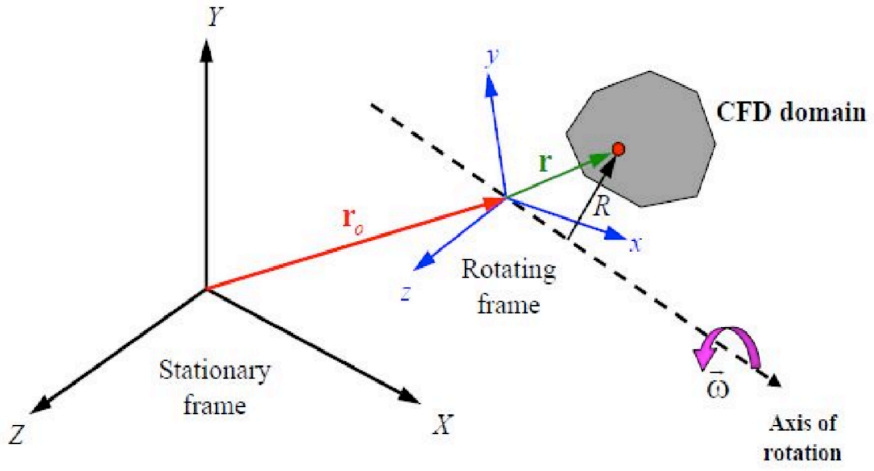

Figure n°5: Computational domain, stationary and rotating reference frames [1]

This model is composed of two reference frame. The rotating one will be defined by x,y,z with a constant angular velocity $\vec{\omega}$ relative to the second reference frame, stationary, defined by X,Y,Z. Each point of the computational domain (in our case the fluid) is defined by a vector $\vec{r}$, which is defined from the origin of the rotating frame. Knowing this, each fluid element velocity $\vec{v}_r$ can be defined in the rotating frame by:

$$\vec{v}_r = \vec{v} - \vec{u}_r \tag{9}$$

Where $\vec{u}_r$ is the velocity relative to the rotating reference frame:

$$\vec{u}_r = \vec{\omega} \times \vec{r} \tag{10}$$

And $\vec{v}$ is the absolute velocity.
With the formula above it is now possible to write and solve the equations of conservation in two different ways, function of relative or absolute velocity. In function of relative velocity, the

formulation is as follows:
Conservation of mass:

$$\frac{\partial \rho}{\partial t} + \nabla . \rho \vec{v}_r = 0 \tag{11}$$

Conservation of momentum:

$$\frac{\partial}{\partial t}(\rho \vec{v}_r) + \nabla . (\rho \vec{v}_r \vec{v}_r) + \rho(2\vec{\omega} \times \vec{v}_r + \vec{\omega} \times \vec{\omega} \times \vec{r}) = -\nabla p + \nabla . \bar{\bar{T}}_r + \vec{F} \tag{12}$$

Conservation of energy:

$$\frac{\partial}{\partial t}(\rho E_r) + \nabla . (\rho \vec{v}_r H_r) = \nabla . (k \nabla T + \bar{\bar{T}}_r . \vec{v}_r) + S_h \tag{13}$$

Using this formulation and because of the change of reference frame, Coriolis acceleration and centripetal acceleration are added in the conservation of momentum equation. It can also be noticed that conservation of energy is in terms of relative internal energy E_r and relative total enthalpy H_r, defined as follows:

$$E_r = h - \frac{p}{\rho} + \frac{1}{2}(v_r^2 - u_r^2) \tag{14}$$

$$H_r = E_r + \frac{p}{\rho} \tag{15}$$

In function of absolute velocity, the formulation is as follows:
Conservation of mass:

$$\frac{\partial \rho}{\partial t} + \nabla . \rho \vec{v}_r = 0 \tag{16}$$

Conservation of momentum:

$$\frac{\partial}{\partial t}(\rho \vec{v}) + \nabla . (\rho \vec{v}_r \vec{v}) + \rho(\vec{\omega} \times \vec{v}) = -\nabla p + \nabla . \bar{\bar{T}} + \vec{F} \tag{17}$$

Conservation of energy:

$$\frac{\partial}{\partial t}(\rho E) + \nabla . (\rho \vec{v}_r H + p \vec{u}_r) = \nabla . (k \nabla T + \bar{\bar{T}} \vec{v}) + S_h \tag{18}$$

Because the entire domain is studied as one rotating frame, the model is the Single Reference Frame (SRF). In this way, the previous equations are solved in all fluid zones. However, with the change in the reference frame, specific boundary conditions have to be set in the entire domain. Wall boundaries, that are moving in accord of the stationary reference frame (turbine blades surfaces), are defined with a no-slip condition, allowing a relative velocity to the rotating reference frame equal to zero. Other wall boundaries, which are not moving in accord of the stationary reference frame (outer walls of the domain), have to be surface of revolution around the rotation axis. They should have a slip condition in order not to shed any vortices.
Periodic boundaries, typical of SRF, are surfaces that must be defined as a rotational periodic boundary about the axis of rotation. Using these boundary conditions, the domain can be defined on 180 degrees with the same resolution as a 360 degrees one, which permits to reduce the computational cost without losing in resolution.[1]

II.2.2) Virtual Blade Model (VBM)

The need to decrease the high computational cost (computational requirements and run time) required with SRF leads to use a simpler but still accurate enough model: the Virtual Blade Model. The validity of this model will be discussed further in this report.

Using the Blade Element theory, this model time-averages dynamics effects of the rotating blades without the need of creating and meshing the actual blade geometry. These effects are simulated with momentum sources terms placed in a rotor disk fluid zone that is characterized by the chord length, the angle of attack, and lift and drag coefficients for different sections along the blade.

A body force in direction x, y and z is created to simulate the effect of rotating blades with VBM. This force acts on an area equal to the swept area of the turbine and is time-averaged over a cycle by the forces calculated with the Blade Element Method (BEM).

This method divides the blade into small sections from the root to the tip. Lift and drag forces will be computed from 2D aerodynamics based on chord length, angle of attack, airfoil type, lift and drag coefficients for each section.
At the inlet boundary, the free stream velocity is used to calculate for each sections le local angle of attack, and the Mach and Reynolds numbers. Then, lift and drag coefficient are interpolated from a look-up table in function of the angle of attack calculated. This look-up table contains the values lift and drag coefficients as a function of angle of attack, Reynolds number and Mach number. It can be created based on experiment data, simulation data from a 2D segment of the airfoil or by modeling a 3D blade span using high fidelity numerical model under the same operating condition. In our case, the look-up table was created using this last method, with a SRF simulation.

Hence, lift and drag forces are calculated for each blade sections using the following equation:

$$F_{L,D} = C_{L,D}(\alpha, Ma, \mathrm{Re})\, c(r/R).\frac{\rho V_{tot}^2}{2} \tag{19}$$

Where $C_{L,D}(\alpha, Ma, \mathrm{Re})$ are lift or drag coefficients, ρ is the fluid density, $c(r/R)$is the chord length and V_{tot} is the velocity of the fluid relative to the blade. $c(r/R)$ depends on the shape of the blade and is provided by the manufacturer.

Then, lift and drag forces are averaged over a full turbine calculation to calculate the source term at each cell in the numerical discretization with these two equations:

$$F_{L,D_{cell}} = N_b . \frac{dr\, r\, d\theta}{2\pi r} . f_{L,D} \tag{20}$$

$$\vec{S}_{cell} = -\frac{\vec{F}_{cell}}{V_{cell}} \tag{21}$$

Where N_b is the number of blade, r is the radial position of the blade section from the center of

the turbine, $d\theta$ is the azimuthal coordinate and V_{cell} is the volume of the grid cell. The flow is updated with these forces and this process is repeated until a converged solution is reached. [1]

II.2.3) Actuator Disk Model

A simpler model was used in this study to improve the VBM, while modeling the hub of the turbine: the Actuator Disk Model (ADM). Indeed, VBM cannot model the hub because the lift would be zero at each sections but the drag would be relevant. Nonetheless, the hub must be modeled to have a physical wake of the fluid behind the turbine, especially to study an array of turbine.

The hub will therefore be represented as a thin porous media with ADM. This media supports a pressure jump, but the velocity remains continuous. A stream tube represents the fluid passing through the media.
Respecting figure 6, U_∞ and p_∞ are respectively the free stream velocity and the pressure, upstream the disk, u_1 and p_1 the velocity and the pressure on the disk, and u_2 the velocity downstream the disk, where the pressure has reached again its initial value p_∞

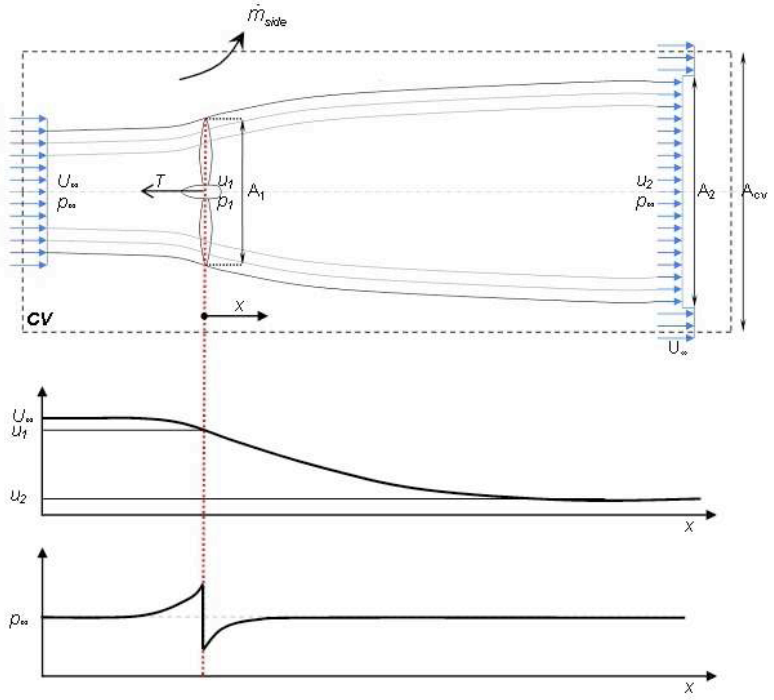

Figure n°6: Stream tube enclosing the rotor in the actuator disk theory [3]

The actuator disk induces a velocity variation, which must be superimposed on the free-stream velocity. This variation is given thanks to the factor 'a', which is called the axial flow induction factor. Hence, the velocity at the disk respects the equation:

$$u_1 = U_\infty(1-a) \tag{22}$$

This velocity can also been written, according to Froude's theory,

$$u_1 = \frac{1}{2}(U_\infty + u_2) \tag{23}$$

Combining these two equations leads to:

$$u_2 = U_\infty(1-2a) \tag{24}$$

Then the pressure jump Δp can be expressed, using Bernouilli's law, with ρ the density of the fluid:

Upstream of the disk: $$p_\infty + \frac{1}{2}\rho U_\infty^2 = p_1 + \frac{1}{2}\rho u_1^2 \tag{25}$$

Downstream of the disk: $$p_1 - \Delta p + \frac{1}{2}\rho u_1^2 = p_\infty + \frac{1}{2}\rho u_2^2 \tag{26}$$

From these two equations, the pressure jump is defined with equation (27):

$$\Delta p = \frac{1}{2}\rho(U_\infty^2 - u_2^2) \tag{27}$$

The power extracted by the disk is defined by:

$$P_e = F_1 u_1 \tag{28}$$

with F1 the force applied on the disk.
This force can also been expressed as following:

$$F_1 = \Delta p A_1 \tag{29}$$

with A1 the area of the disk.

As a consequence, from equations (27), (28) and (29) , the power extracted by the disk is:

$$P_e = \frac{1}{2}\rho(U_\infty^2 - u_2^2)A_1 u_1 \tag{30}$$

Finally, the actuator disk extracts a power as described on equation (31), from equations (22), (24) and (30) :

$$P_e = \frac{1}{2}\rho U_\infty^3 A_1 4a(1-a)^2 \tag{31}$$

Knowing that the total power available is :

$$p_{total} = \frac{1}{2}\rho U_\infty^3 A_1 \tag{32}$$

The efficiency defined by :

$$\eta = \frac{P_e}{P_{total}} \tag{33}$$

can be written:

$$\eta = 4a(1-a)^2 \tag{34}$$

According to [9], this efficiency must respects the Betz's limit on the maximal power that can be extracted:

$$\eta = \frac{P_e}{P_{total}} = \frac{16}{27} \approx 0.593 \tag{35}$$

In Fluent, the hub is modeled by a porous media, which is an added momentum sink in the governing momentum equation.
It contributes to the pressure jump, and can be determined for an homogeneous porous media with equation…:

$$S = -(\frac{\mu}{\alpha}u + C_2\frac{1}{2}\rho u^2) \tag{36}$$

where S is the source term, ρ the density of the fluid, μ the dynamic viscosity of the fluid, u the velocity of the fluid normal to the media, α the face permeability of the media and C2 the pressure jump coefficient.
Two terms compose this equation: a viscous loss term and an inertia loss term.

The pressure jump, which is due to the kinetic energy change of fluid across the media, is also defined as follows:

$$\Delta p = -S\Delta m \tag{37}$$

where Δm is the thickness of the porous media.

Using equations (36) and (37) the pressure jump can be written:

$$\Delta p = (\frac{\mu}{\alpha}u + C_2\frac{1}{2}\rho u^2)\Delta m \tag{38}$$

The coefficients $\frac{1}{\alpha}$ (viscous resistant coefficient) and C_2 (inertial resistant coefficient) permit to describe the porous media in Fluent, and has to be determined. [3]
Based on certain efficiency, the induction factor 'a' is determined (equation (34)). Then, u_1, u_2 and Δp can be calculated thanks to equations (22), (24) and (27) .
Once Δp known, the two coefficients above can be determined using equation (38), while taking u1 for the velocity u .

This method will be used and described more precisely later in this report to model the hub in VBM.

III) STUDY OF SINGLE TURBINE CONFIGURATION: DOE REFERENCE MODEL 1

III.1) Single Rotating Reference Frame (SRF)

III.1.1) Arguments to redraw the mesh

After analyzing the previous work by a previous researcher in the lab, Mr. Arthur Cerisola, it became apparent that the root region of the DOE Model 1 blade was responsible for significant vorticity shedding into the wake that made the simulation converge slowly and increased the uncertainty, while contributing very little to the predicted power. It was therefore decided to remesh and run simulations with a modified domain that excludes the root region, in order to quantify this loss of power. Several criteria have been chosen to have an optimized redrawn mesh. The first one was the lift and drag forces measured from the simulation. The second one was the shape of the blade sections, responsible for separation or attached flow. The last one was the vorticity shedding induced by those blade sections.
The part of the blade between blade section 0 and blade section 3 creates very little lift and, as a result, very little power. The shapes of the blade sections are elliptic (Figure 7, 8 and 9), so they are responsible for a lot of separation and so vorticity. (Figure 10).

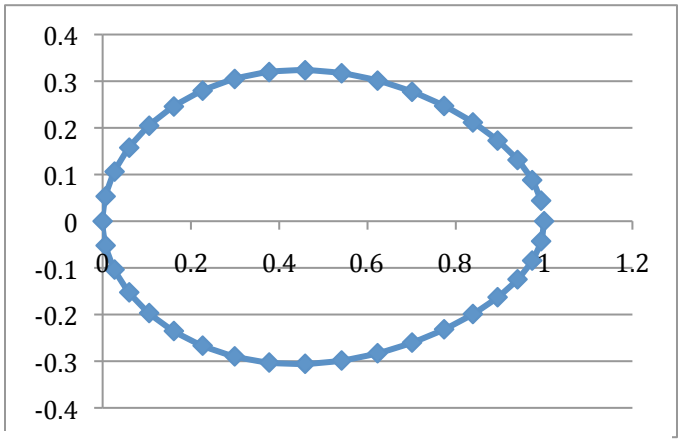

Figure n°7 : Blade section 0 – NACA 60629

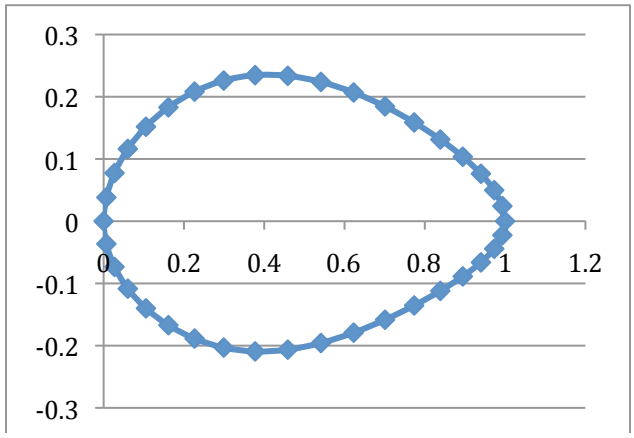

Figure n°8 : Blade section 1 – NACA 60444

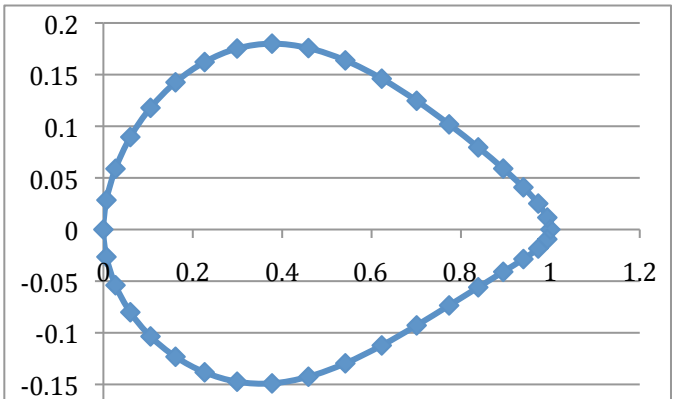

Figure n°9 : Blade section 2 – NACA 60329

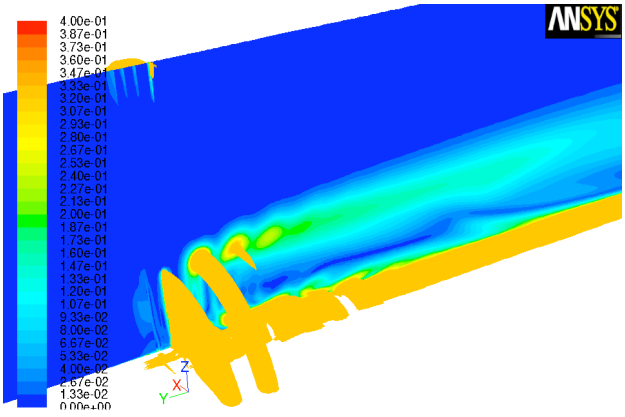

Figure n°10 : Tip and hub vortices – Arthur Cerisola's case

All these reasons have led us to redraw the mesh and increasing the size of the hub from 1.75m to 2.8m. In this way the previous root of the blade is "absorbed" in the new hub allowing blade 3 to be the first modeled section.

The base of this new mesh is Arthur Cerisola's one. The first thing done was deleting the parts that were going to be absorbed by the new geometry. The hub and the blade section 0, 1, 2, 3 have been deleted. (In black on figure 11).

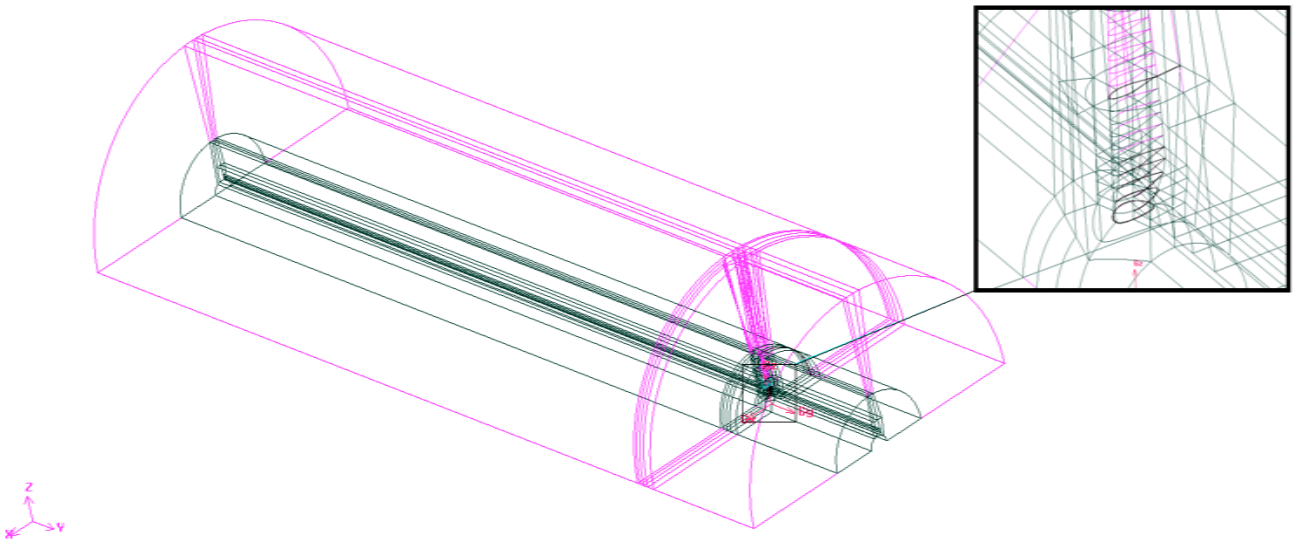

Figure n°11: Arthur Cerisola's mesh – Elements to redraw

Once this was done, the major issue was to redraw a new hub with a radius of 2.8 meters and to integrate it in the C-mesh that was already defined all around the blade. It was imperative to keep the geometry of the C-mesh in order to keep the control on the near-wall regions where the turbulent boundary layer will be developed. In this redrawn mesh the wall function approach is kept to have a good accuracy of the flow field near the blade. This permits to have the most precise value of power extracted by the blade.
Also to lower the skewness without increasing the number of element, many faces that were twisting around the blade have been divided in several faces. This way it is easier to mesh the faces properly because they are more planar. The mesh is more ordered on the faces and, as a result, the skewness is better.

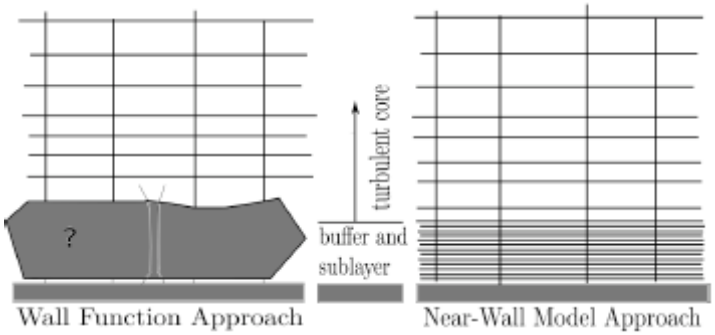

Figure n°12: Two approaches for near wall region meshing

The base of the near-wall function is a semi empirical formula that is use to solve the viscous sub layer and buffer layer. Contrary to near-wall modeling approach that uses a more refined mesh near the wall, these functions allow fewer cells reducing computational cost. The near wall function is still able to predict the mean velocity profiles, flow detachment, dissipation mean shear at the wall, etc. (Figure 12).

After the boundary conditions have been set, in accord with the SRF model. The mesh has 9 767 825 elements and a maximum skewness of 0.83. (Figure 13).

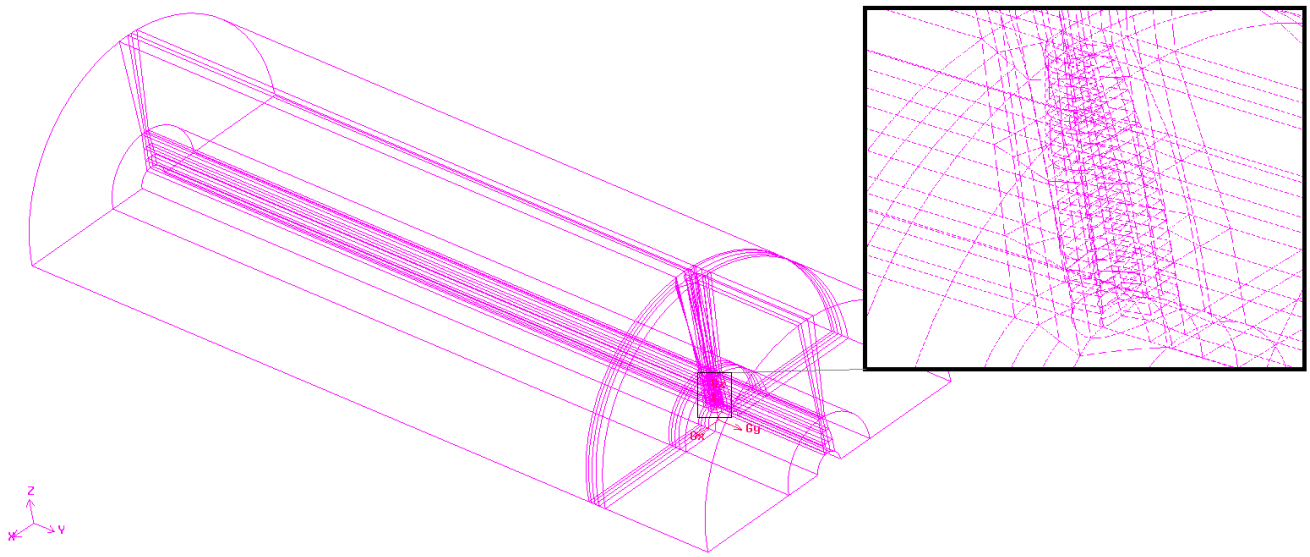

Figure n°13: Final mesh – Hub radius = 2.8

III.1.2) Results from the SRF Simulations: lift and drag coefficients

The lift and drag coefficients from the SRF simulations described in the previous section have been extracted in order to use them as input into the Virtual Blade Model (VBM) simulations.

First, two forces are reported from the SRF simulations for each section of the blade, as defined on the geometry (see appendix): X-force and Y-force. These forces are perpendicular and parallel respectively to the free stream velocity. These two forces are then used to calculate lift and drag forces using equations (39) and (40).

$$L = Y\cos(\varphi) + X\sin(\varphi) \qquad (39) \qquad D = Y\sin(\varphi) - X\cos(\varphi) \qquad (40)$$

Lift and Drag forces are respectively perpendicular and parallel to the relative velocity (figure14), which is expressed:

$$V_{rel} = \sqrt{U_\infty{}^2(1-a)^2 + \omega^2 r^2(1+a')^2} \qquad (41)$$

Where $U_\infty(1-a)$ is the local velocity and ωr(1+a') is the net tangential flow velocity experienced by the blade.

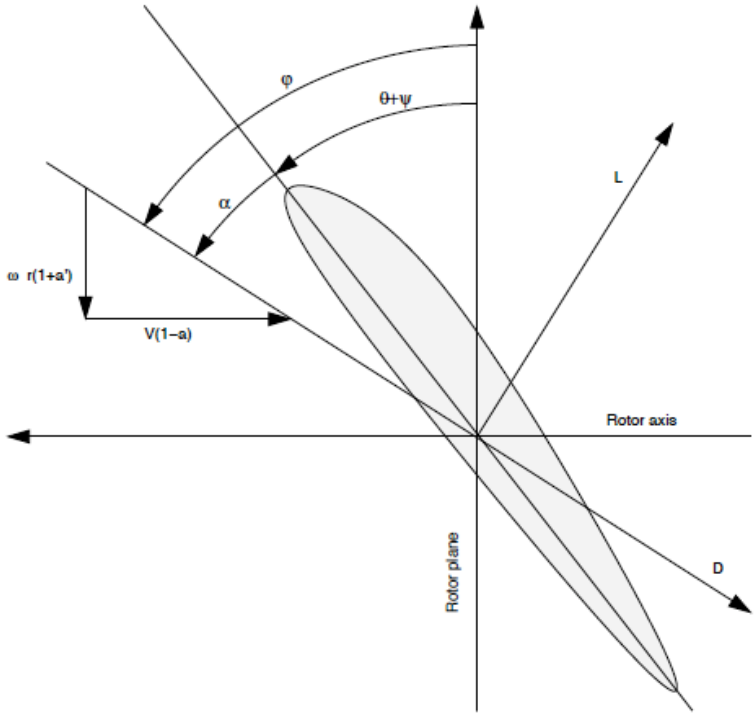

Figure n°14: Angle and velocity convention (with V=U∞)

As shown on figure 14, the angle φ can be expressed:

$$\varphi = \tan^{-1}\left(\frac{U_\infty(1-a)}{\omega r(1+a')}\right) \tag{42}$$

In our case, we consider a' equal to zero. Nonetheless, the local velocity cannot be consider equal to the free stream velocity, and had to be determined by observing the velocity contours and vectors near the blade at different sections along the blade span (figure 15). The magnitude of the local velocity is the value for which the velocity vectors in close proximity to the blade have the same direction as the free stream velocity.

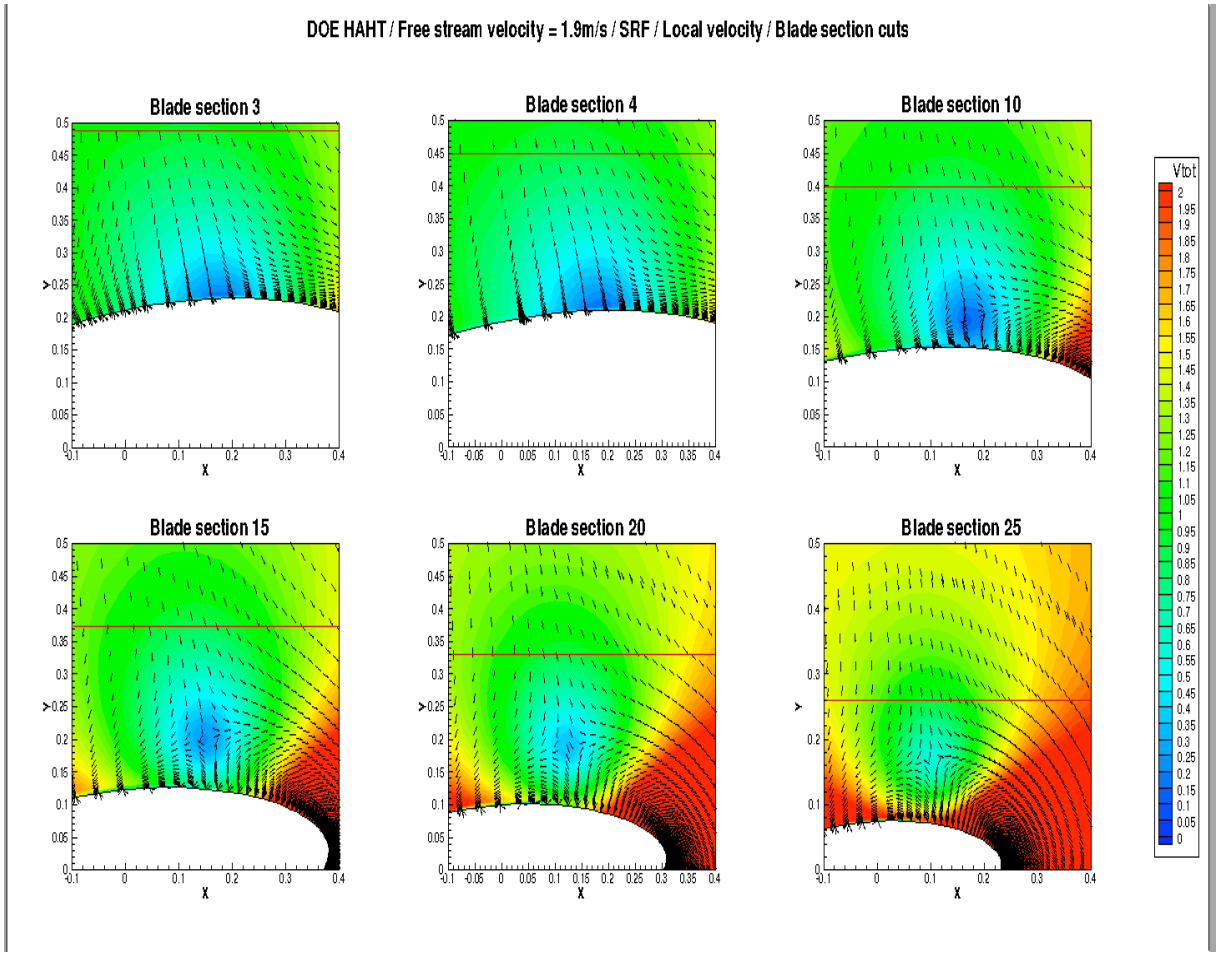

Figure n°15: Determination of local velocity

The local velocity is found to be equal to 1.2m.s^{-1}.

For each section, the angle of attack α can then be calculated using equation 42 :

$$\alpha = \varphi - \theta - \psi \tag{43}$$

Where θ is the collective pitch angle (here equal to zero) and ψ is the local twist angle (provided by the geometry of the blade).

Knowing lift and drag forces, lift and drag coefficient are calculated as following:

$$C_{L,D} = \frac{L,D}{\frac{1}{2}\rho * c(r) * s * V_{rel}{}^{2}} \tag{44}$$

Where c(r) is the chord of the section, s is the width of the blade segment span used in the discretization of the blade for lift and drag calculations and is equal to 0.3m, and ρ the density of the fluid.

Lift and drag coefficients are shown on figures 16 and 17, as a function of the angle of attack and of the position along the blade span, respectively, for two simulations with different turbulence models: Spalart Allmaras and K-ω.

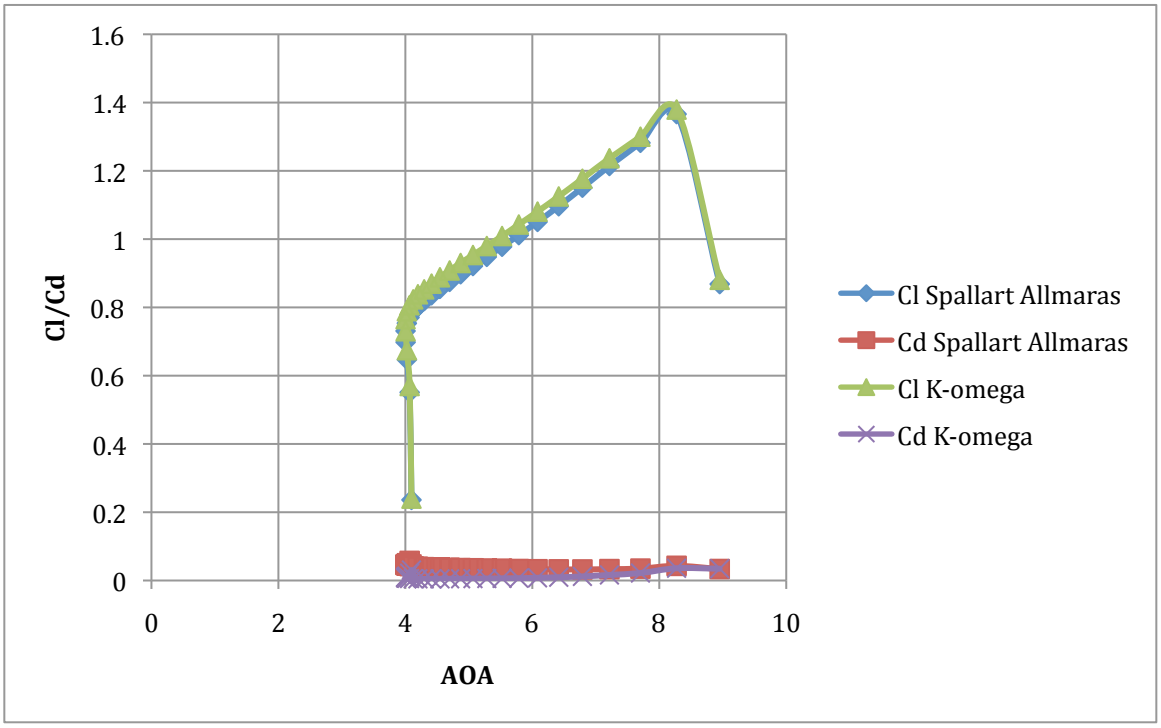

Figure n°16: Lift and drag coefficients in function of angle of attack

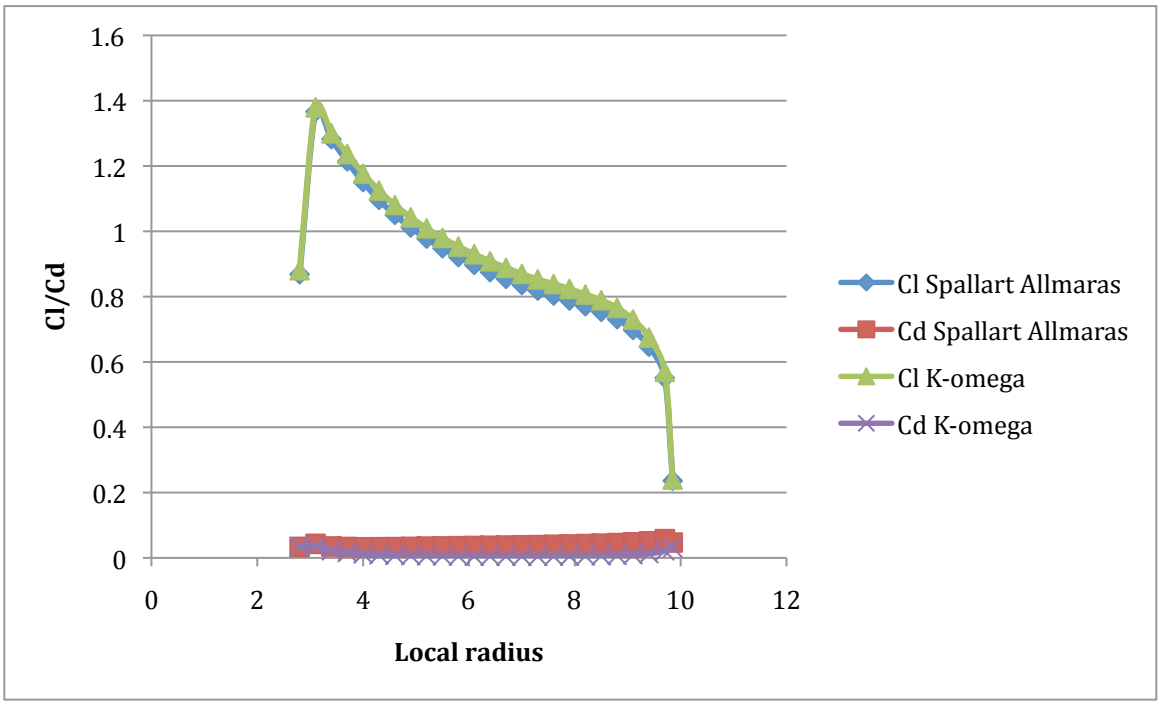

Figure n°17: Lift and drag coefficients in function of the position along the blade

Lift coefficients are slightly higher for the K-ω model than for the Spalart Allmaras, and drag coefficients are lower for K-ω than for Spalart Allmaras. We can expect a higher power prediction with the K-ω model.

The values of the lift coefficient decrease abruptly at the tip of the blade: this is the tip effect, which is associated with the 3D flow near the edge of the blade span. A strong coherent vortex is created due to this phenomenon as shown on the with the vorticity contours from the SRF simulation (figure 18).

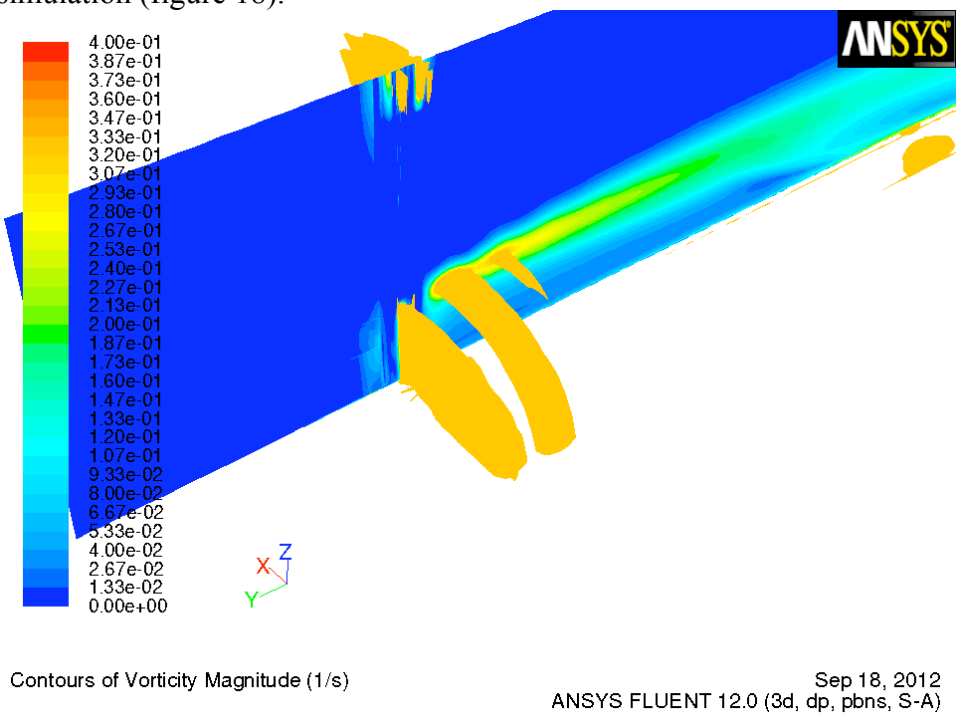

Figure n°18: Tip vortex spiraling from the blade tip in its rotation. The step of the helix described by the vortex is given by the Tip Speed Ratio.

We can also observe a sudden drop of the lift coefficient close to the root. This can be explained by the sudden detachment of the flow, stall induced by the blunt geometry of the blade, that produces a precipitous decrease in lift and increase in drag as the pressure on the suction side increases from the trailing edge to near the leading edge.

Taking into account these last two observations, the choice to keep values of lift and drag coefficients only for angles of attack from 4.00° to 7.70° has been made to create the look-up table needed for VBM. Outside this range of angles of attack, the values do not seem representative of the normal flow around the blade profiles. Tip effects and root detachment are accounted by the VBM model in a way independent of the angle of attack dependency of lift and drag.

III.1.3) Results from the SRF Simulations: Torque and Power calculations

The X component of the hydrodynamic force contributes to creating torque on the blade rotational axis. This torque is calculated for each section defined by the geometry, based on the computed force (in our case force applied on the vector (1,0,0)), and the center of pressure directed by z-axis in the plane including the blade and whose normal vector is collinear to x-axis (vector (1,0,0)).
As a consequence, the expression of the torque for section 'i' is the following:

$$T_i = X_i * z_i \tag{45}$$

Where T_i is the torque of the i-th section of the blade, X_i the X-force experienced by this section, and z_i its center of pressure defined as above.

Then, the total torque created is the sum of each section torque:

$$T = \sum_i T_i \tag{46}$$

and the power P extracted by the blade is:

$$P = 2 * T * \omega \tag{47}$$

with ω the rotor angular velocity (rad.s^{-1}). The factor 2 represents the fact that the real turbine is composed of two blades: the power produced by only one blade is T*ω.

Knowing how to calculate the power, comparison with previous studies on the DOE reference model 1 can be made, to see the quality of the SRF-mesh used in this study.
Two previous works were used:

- 2D simulation from NREL laboratory
- 3D NREL [11], which modeled the blade in 3D using another CFD package similar to SRF that used periodic boundary conditions (STAR CCM +).
- The mesh created by Mr. Cerisola [5] –with the hub- was also refined in the region near the hub.

The settings of these simulations are described on table1 :

Material	Seawater
Turbulence model	SST K-ω
Turbulence intensity	5%
Turbulence length scale	1m
Free-stream velocity	1.9m/s
Rotor speed	11.5rpm
Blade pitch	0deg

Table n°1: Operating conditions

The turbulence intensity, I, is defined as the ratio of the root-mean-square of the velocity fluctuations, u', to the mean flow velocity, $\overline{u}$.

$$I = \frac{u'}{\overline{u}} \tag{48}$$

The turbulence length scale is a physical quantity related to the size of the large eddies that contain most of the energy in turbulent flows [13].

The different power extracted by the blade for these simulations are summed up in table 2

	Power (kW)
2D NREL	496
3D NREL [11]	504
Cerisola refined mesh (with root)	523
SRF mesh (without root)	511

Table n°2: Power comparison

The efficiency, defined by:

$$\eta = \frac{P_{extracted}}{P_{available}} = \frac{P_{extracted}}{\frac{1}{2}\rho S U_{\infty}^{3}} \tag{49}$$

is close to 50% for these simulations. This value is considered to high and most likely not representative of real efficiency values in experiments or the field. We can assume these simulations to over-predict the power extracted by the blade.

The gap between power results from the different simulations was calculated (table 3)

Relative error (%)	**2D NREL**	**Reference X**	**Cerisola refined mesh**	**SRF mesh**
2D NREL	X	X	X	X
3D NREL [11]	1.61%	X	X	X
Root-region refined mesh	5.44%	3.77%	X	X
SRF mesh	3.02%	1.39%	2.29%	X

Table n°3: Relative error of power between two simulations (with reference taken in column)

The biggest gap is between the 2D NREL simulation and the root-region refined mesh: 5.44%, somewhat high but still acceptable.
The gap between the root-region refined mesh and the mesh excluding the root is particularly interesting: it shows that cutting the root, we are only losing 2.29% of power extracted by the turbine. This confirms the assumption that the region of the blade near the hub does not produce a big amount of power, and so can be omitted from the computational domain.

The torque produced by each sections of the blade is shown on figure 19, for the SRF mesh, using the two different turbulence methods sum up in table 4.

The other operating conditions are the ones previously described on table1

	Spalart Allmaras	K-ω SST
Pressure-velocity coupling scheme	SIMPLE	SIMPLE
Discretization of gradient	Green-Gauss Node Based	Green-Gauss Node Based
Discretization of pressure	2nd order	2nd order
Discretization of momentum	QUICK	QUICK
Modified turbulent viscosity	QUICK	-
Turbulent kinetic energy	-	1st order upwind
Specific dissipation rate	-	1st order upwind

Table n°4: Solution method

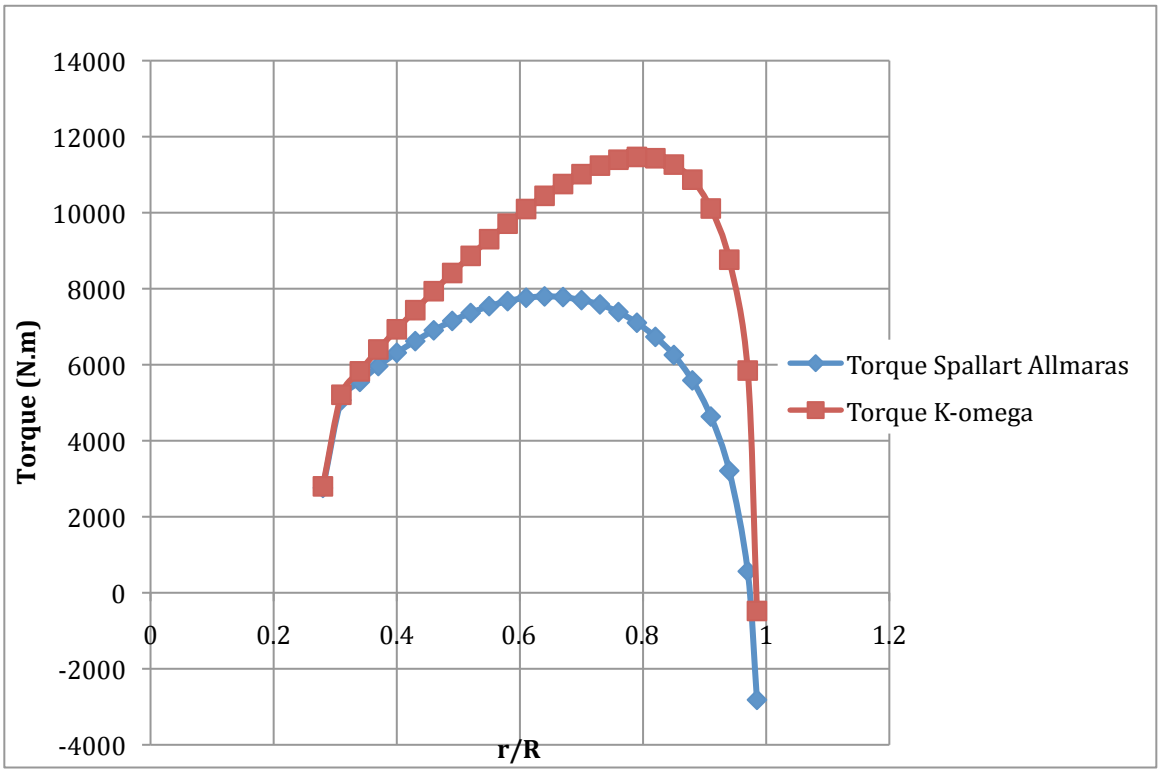

Figure n°19: Torque in function of normalized radius of the blade

The torque calculated with the K-ω SST simulation is a lot higher than with Spalart Allmaras. This confirms the prediction of higher efficiency made above (50.24% for this simulation). The power calculated with the Spalart Allmaras simulation, 351kW, corresponds to an efficiency of 34.47%. This efficiency is more realistic compared to the 511kW of power calculated with the K-ω SST simulation.

Close to the tip of the blade, we can see that the torque is negative for both simulations: power is not extracted from the last section due to the tip effect.

III.1.4) Results from the SRF Simulations: Velocity Profiles

Knowing the differences of power between de Spalart-Allmaras turbulence model and the K-ω turbulence model it is interesting to look at the velocity contours differences in SRF.

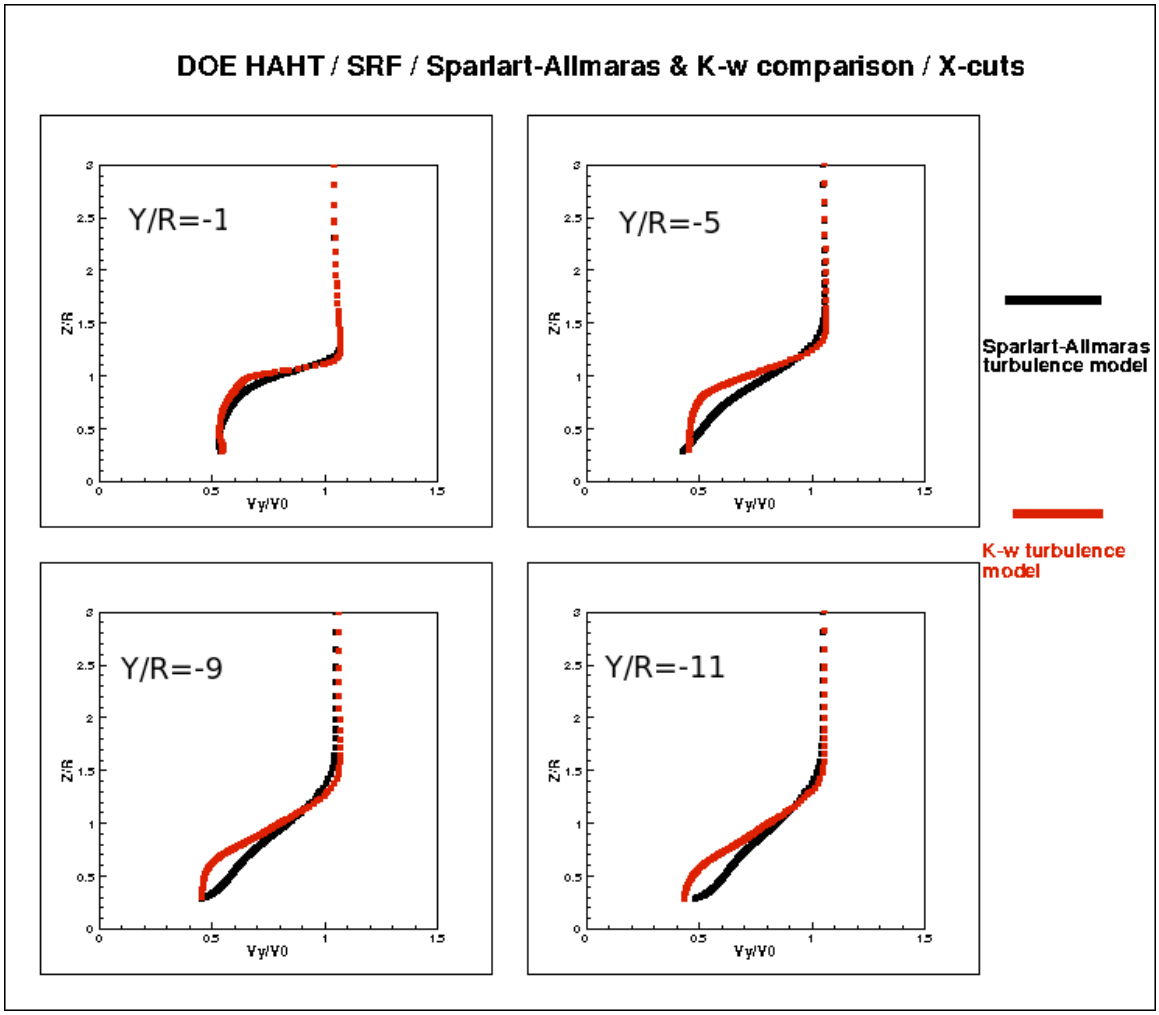

Figure n°20: Comparison of SRF velocity contours at four distances downstream the turbine for the Spalart Allmaras and the K-ω turbulence model

This chart represents the normalized velocity along the y direction (flow direction) at different section in function of the z direction. On each chart, the velocity profiles for the Spalart-Allmaras turbulence model and the k-ω turbulence model are represented.
Knowing that both turbulence models are using a near-wall function approach, we can notice that the velocity deficit is quite similar close to the blade. In contrast, the wake velocity deficit is higher in the K-ω turbulence model, which is consistent with the observation that the power extracted by the blade predicted with this model is higher. It can also be noticed that for the k-ω turbulence model there is a Vy/V0=0 tangent at the root and that for the Spalart-Allmaras turbulence model there is a Z/R=0 tangent at the root.

III.2) Virtual Blade Model (VBM)

III.2.1) Without the hub

In order to compare with the SRF model and determine the accuracy of the VBM simulation on the DOE Reference Model 1 turbine, a new mesh has been created, whose dimensions respects the previously described SRF mesh.
The VBM mesh, built with GAMBIT (ANSYS, Inc. Cannonsburg, PA.) software, is defined in figure 21.

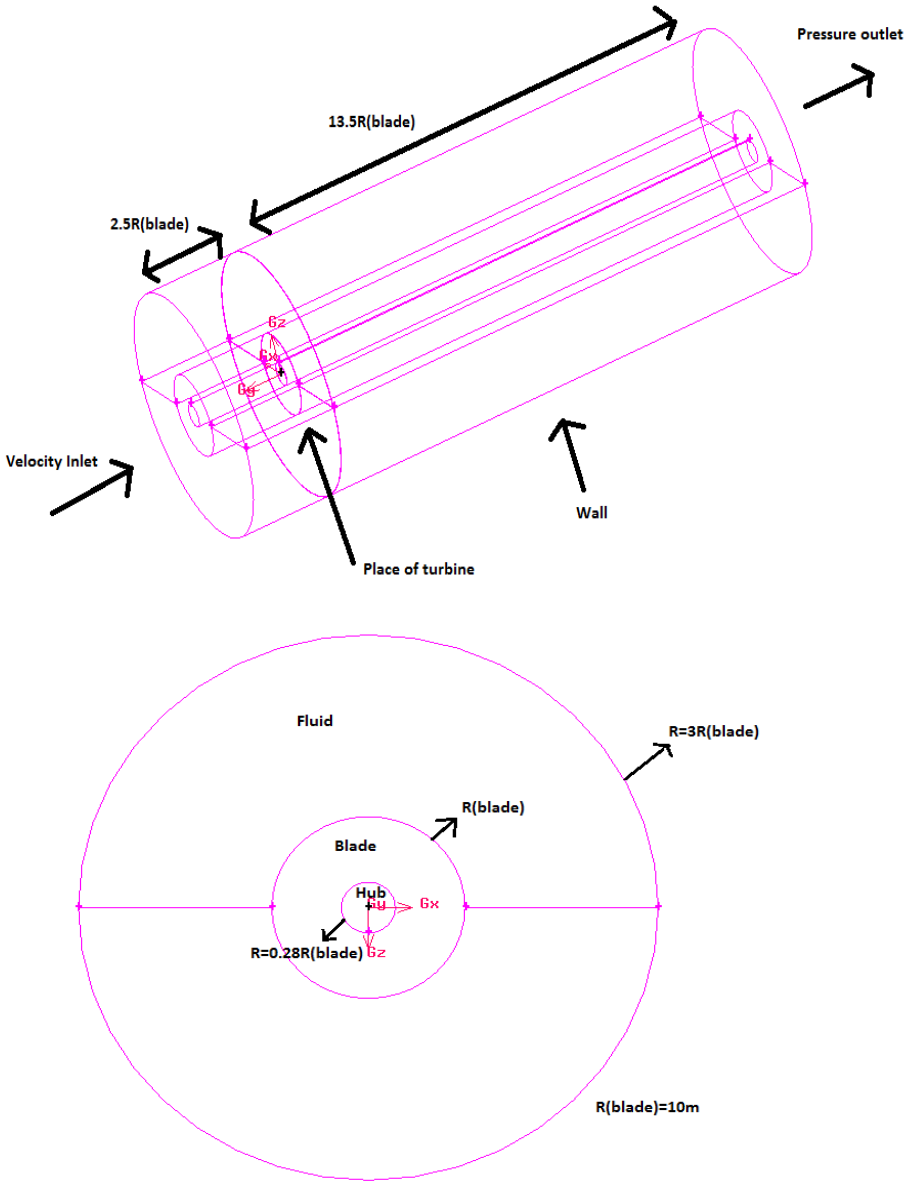

Figure n°21: Geometry of the VBM mesh for the DOE reference model 1

The hub has a radius of 2.8m, and two circles with radius equal to 2.8m and 10m define the blade respectively (from the root to the tip). The mesh is structured: the elements are hex/wedge.
Two sections, spaced by 12cm, have been created near the blade in order to have a finer mesh in the blade vicinity. A 'rot_face' was created to respect the needs of VBM inputs. A volume called 'fluid_rot' was also created for the same reason: this is where momentum sources are placed.

First, the hub has been excluded from the VBM mesh so that the power and the wake velocity profiles could be directly compared to the results from the SRF simulation. This mesh is composed of 1 849 692 elements. Then, a second mesh was created taking including the hub of the turbine. The hub was modeled using the ADM theory, and is particularly important to study different configurations of an array of turbine. This second mesh is composed of 2 195 215 elements.

Once the mesh was created, several simulations were launched.
The different inputs to run a VBM simulation are the following:

- Read the mesh.
- Compile User Defined Functions (UDFs) provided by the VBM tutorial of ANSYS FLUENT.
- Read a VBM scheme, also provided by ANSYS FLUENT.

An UDF is a C-programmed function, which can be used with FLUENT in order to enhance the standard features of the commercial package.

The VBM settings window (provided by the scheme) is shown on figure 22.

Figure n°22: VBM settings

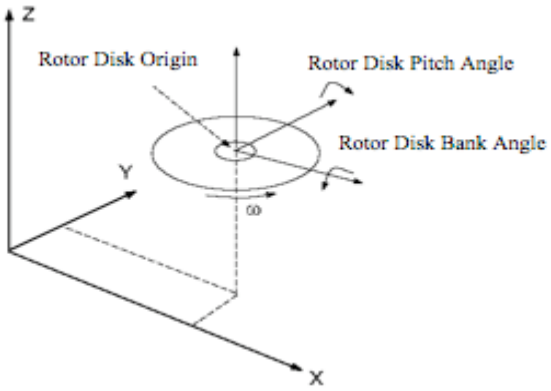

The bank angle (define on figure 23) is set to 90° because the turbine is a horizontal axis one. The number of rotor zone can be changed up to 10, so that an array of turbines can be studied. In that case, all rotor zones do not have to be activated together, and specific configurations can also be studied. The pitch angle is 0° in our study. The flap has been designed for applications to helicopter rotor aerodynamics.

Figure n°23: VBM angles convention

As the VBM enable the user to define only 20 sections of the geometry of the blade, 5 sections had to be deleted compared to the 25 sections calculated by the SRF simulation, described above (appendix X). A methodology has been adopted to choose the right sections to omit. Taking into account the fact that VBM interpolates between two sections to calculate the lift and drag forces, and that these forces are functions of the angle of attack (from the look-up table), the difference between the angles of attack of two successive sections has been observed. Then, a section can be omitted if its difference of angle of attack with the next one is low.
This method leads us to use sections 3 to 27 without sections 15; 17; 19; 21 and 23 to define the blade in VBM. Once the sections were chosen, the parameters of the turbine can be input in the tab 'geometry'; for each section, the position along the blade (radius of the section over blade radius), the chord length, the twist angle and also the look-up table (lift and drag coefficients in function of angle of attack) are set. The twist angle is negative due to convention sign.

The look-up table from the Spalart Allmaras SRF simulation -described on appendix X- was built as shown on figure 24. Another table, based on K-ω SRF simulation, has also been used in the VBM simulations and comparisons of the results with both Cl-Cd tables is presented below.

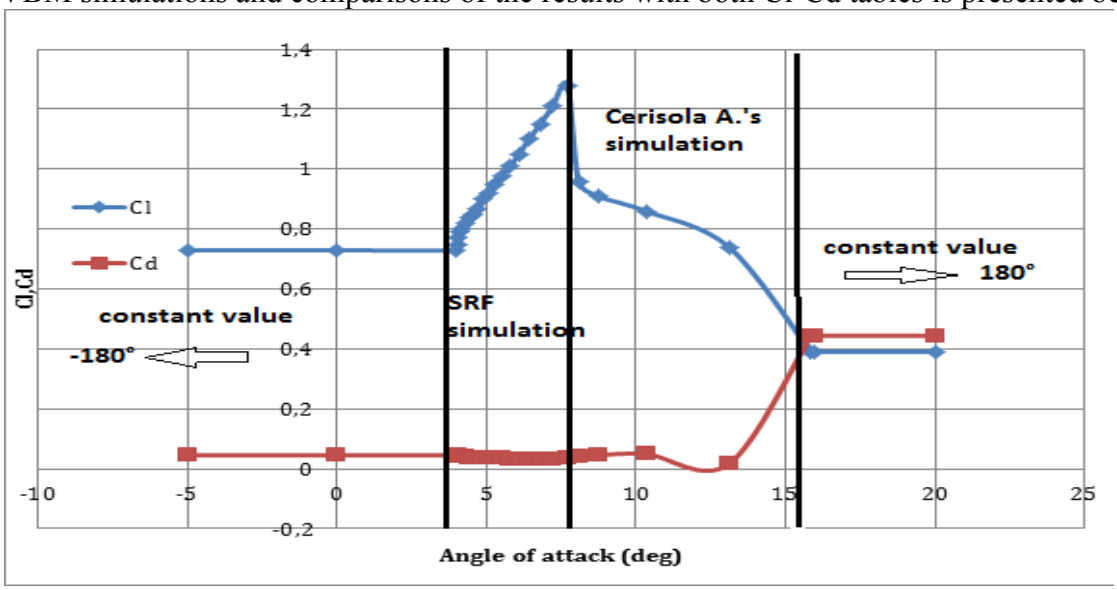

Figure n°24: Lift and drag coefficients in function of angle of attack in VBM table

The table has to be defined for angles of attack from -180° to 180°.

- From 4.00° to 7.70°, the values of lift and drag coefficients come from the previous SRF simulation.
- From 7.70° to 15.86°, the values come from Mr. Arthur Cerisola's simulation. The jump can be explained by the difference of NACA profile for the lower sections, and the fact we are getting closer to the root of the blade, where the chord length evolves significantly. The goal of these values is to 'help' the convergence.
- Under 4.00° and over 15.86°, a reference value has been set, which corresponds to these last defined values.

According to these assumptions, the validity of a VBM simulation can be first observed with the range of angles of attack. The angles of attack should be included between 4.00° and 7.70° to consider that the simulation uses right coefficients to calculate the thrust, torque and power.

The tip effect has been defined to take into account the phenomenon induced by an increasingly strong secondary flow around the tip of the blade. Indeed, in VBM, local lift and drag forces are computed assuming 2D flow, without accounting for this 3D phenomenon. As a consequence, the decrease of the lift near the tip of the blade is not represented. To describe it, a tip effect percentage is set as an input, which is a percentage of the blade where the blade actually produces lift. Outside this percentage (1 –tip effect %), the blade sections corresponding to that area do not produce lift, but do produce drag forces.

Several simulations have been launched to understand the tip effect. It has been observed that Fluent does not interpolate between two sections to calculate the lift and drag forces. Having the position for the tip effect between two sections would therefore not change the value of the power calculated, because the lift for the entire section would be added to the total blade values in its totality, and not just for the fraction of the section that is within the limit given by the tip effect parameter. For example, if the last section of the blade goes from 0.98 to 1.00 radius along the blade, any value of tip effect parameter larger than 98% would produce the same power and torque, as it would include the lift from that section in its entirety.

The inlet velocity (free stream velocity) is set to $1.9 m.s^{-1}$ and the rotor angular speed is 11.5rpm. The turbulence is specified with an intensity of 5%, and a length scale of 1m. The solution method is the same as SRF simulation (table 4).

In order to validate the VBM simulations, the range of angles of attack is checked: it should be between 4.00° and 7.70 because of the structure of lift and drag coefficient table used. This range of angles of attack is shown table 5, for the different VBM simulations studied.

Turbulence model	Material	Tip effect	Minimum angle of attack	Maximum angle of attack
Spalart Allmaras	water	96%	4.32°	6.74°
Spalart Allmaras	water	98%	4.33°	6.56°
Spalart Allmaras	seawater	96%	4.31°	6.73°
Spalart Allmaras	seawater	98%	4.38°	6.52°
SST K-ω	water	96%	3.96°	6.85°
SST K-ω	water	98%	4.11°	6.45°
SST K-ω	seawater	96%	3.96°	6.85°
SST K-ω	seawater	98%	4.01°	6.20°

Table n°5: Range of angles of attacks for VBM simulations

The range of angles of attack is acceptable, even for the two SST K-ω simulations with a tip effect of 96%, which have a minimum angle of attack of 3.96°. This angle is indeed really close to the 4.00° needed.

The first result from the VBM simulations refers to the computational methodology: the effect of the change of turbulence model. Two simulations were run with exactly the same settings (look-up table, seawater, turbulence intensity 5%, length scale 1m), but with changing the turbulence model. The power extracted with the Spalart Allmaras model is 365kW (η=35.86%), and the one extracted with the SST K-ω model is 315kW (η=30.95%). This shows that either Spalart Allmaras over predicts the power extracted by the turbine, or SST K-ω under predicts this power.
However, the efficiency calculated tends to point towards SST K-ω model under predicting the power because its value is low compared to design calculations for this turbine (the DOE reference model 1).

After the first investigations about SRF and VBM numerical model, comparison between these models can be made.

III.2.2) Modeling the hub

The hub is modeled with ADM theory. The methodology adopted is the one described in II.2.3). Several induction values were taken for the hub region: η=10%, η=20% and η=25%. The porous media, which is used to model the hub, should not take energy from the flow, so the efficiency should be low. Nonetheless, the efficiency has to be high enough to recover a 'flat' velocity profile downstream of the turbine, which means that the velocity downstream the turbine should be continuous from the blade to the hub, or having a smooth transition.

For each efficiency, the axial induction factor has been calculated thanks to equation (34). This gives the possibility to calculate u_1, u_2 and the pressure jump Δp thanks to equations (22), (24) and (27), for several free stream velocities. Using these data, Δp can be expressed in function of u_1. Figure 25 represents Δp in function of u_1 for an efficiency η=20%.

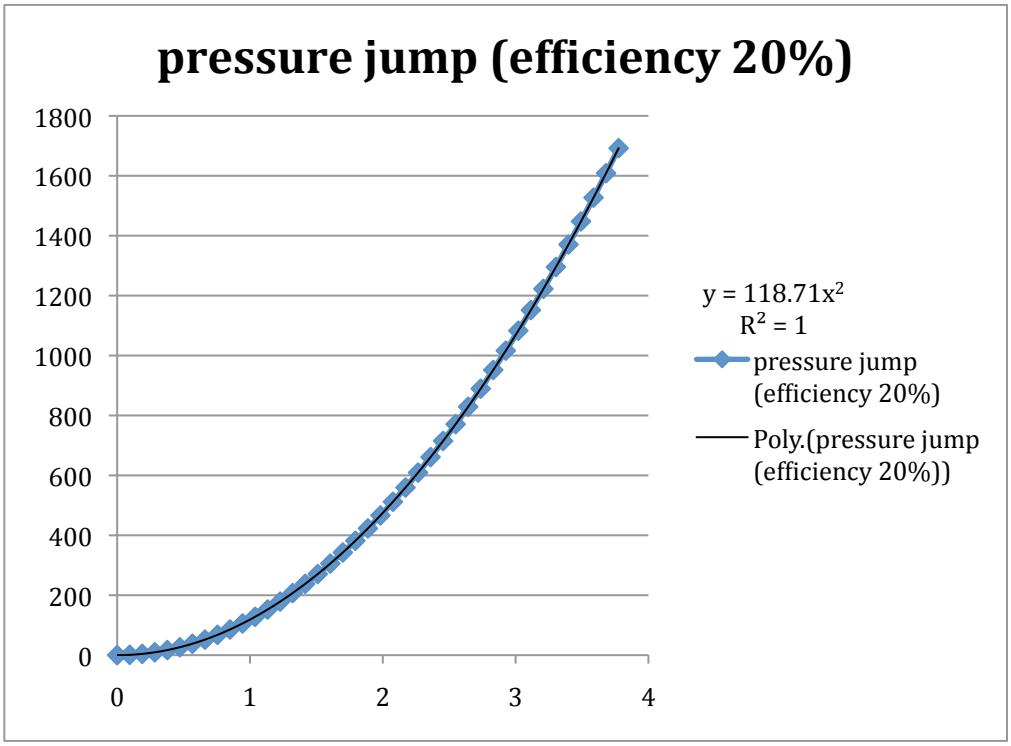

Figure n°25: Pressure jump in function of local velocity for an efficiency of 20%

The pressure jump can be expressed:

$$\Delta p = 0 * u_1 + 118.71 * u_1^2 = K1 * u_1 + K2 * u_2^2 \qquad (50)$$

According to equation (50), we have:

$$\frac{1}{\alpha} = \frac{K1}{\mu * \Delta m} \qquad (51) \qquad \text{and} \qquad C2 = \frac{2 * K2}{\rho * \Delta m} \qquad (52)$$

K1(η=20%)	K2(η=20%)
0.00E+00 $kg.m^{-2}.s^{-1}$	118.71$kg.m^{-3}$

1/α (η=20%)	C2(η=20%)
~0 m^{-2}	1.982067722 m^{-2}

Table n°6: Coefficients allowing to describe the porous zone for an efficiency of 20%

The velocity contours have been observed for each efficiency, for different distances downstream of the turbine (with R equal to one radius: 10m): 1R downstream (red), 4R (green), 6R (navy blue), 8R (sky blue) and 10R (white). The position in abscise is the X-position of the domain, so the hub is from -2.8m to 2.8m and the blade from +/-2.8m to +/-10m.

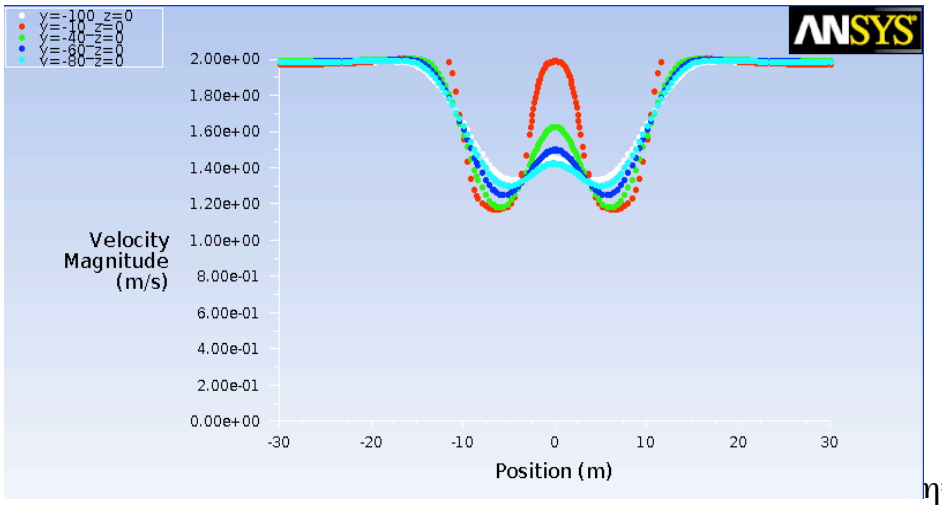

η=10%

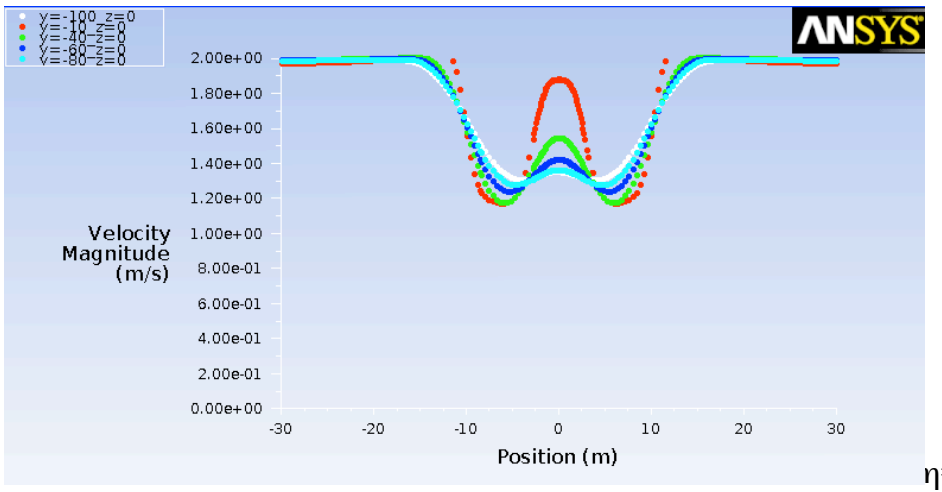

η=20%

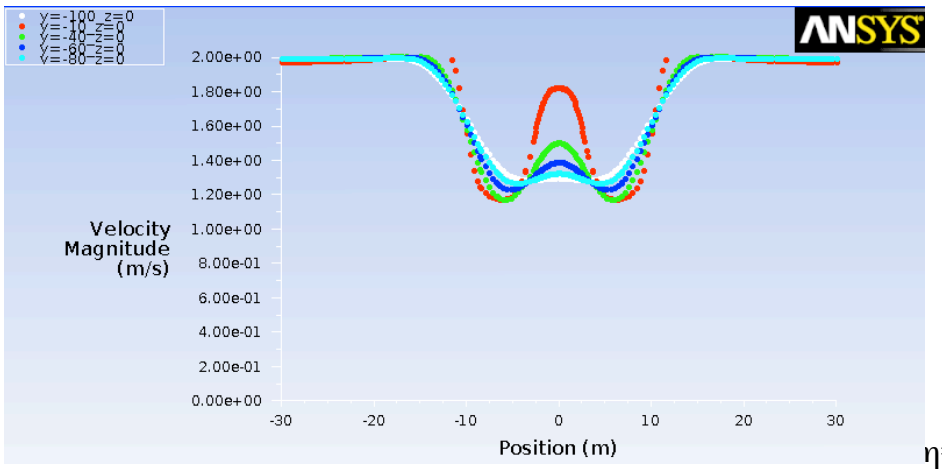

η=25%

Figure n°26: Comparison of velocity magnitude contours for efficiencies modeling the hub of 10%, 20% and 25%

We can see for each case that there is a huge acceleration of the flow just behind the hub (1R downstream), which does not represent what happens in reality. Nonetheless, what interests us while modeling the hub is the far wake of the flow, so this error is not important as long as the far wake velocity is continuous.

For an efficiency of 10%, the velocity contours do not recover a 'flat' profile quick enough. The porous media does not extract enough energy, so the wake of the flow is not well characterized and the speed of the flow behind the hub is too high compared of the velocity behind the blade.

The velocity contours for efficiencies equal to 20% end 25% are quite similar, even if the velocity contours for 25% are recovering a flat shape a little sooner. However, the low acceleration we can see behind the hub, in the far wake for 20% efficiency is acceptable. As a consequence, having an efficiency of 20% seems to be a good compromised between the need of low efficiency and continuous velocity. The viscous resistance and inertial resistant coefficients from an efficiency of 20% will therefore be used to characterized the porous media that models the hub in FLUENT.

The velocity magnitude contours can be shown in a plane perpendicular to the turbine, for the efficiency of 20%, on figure 27 , where we can observe the continuity of the velocity in the far wake.

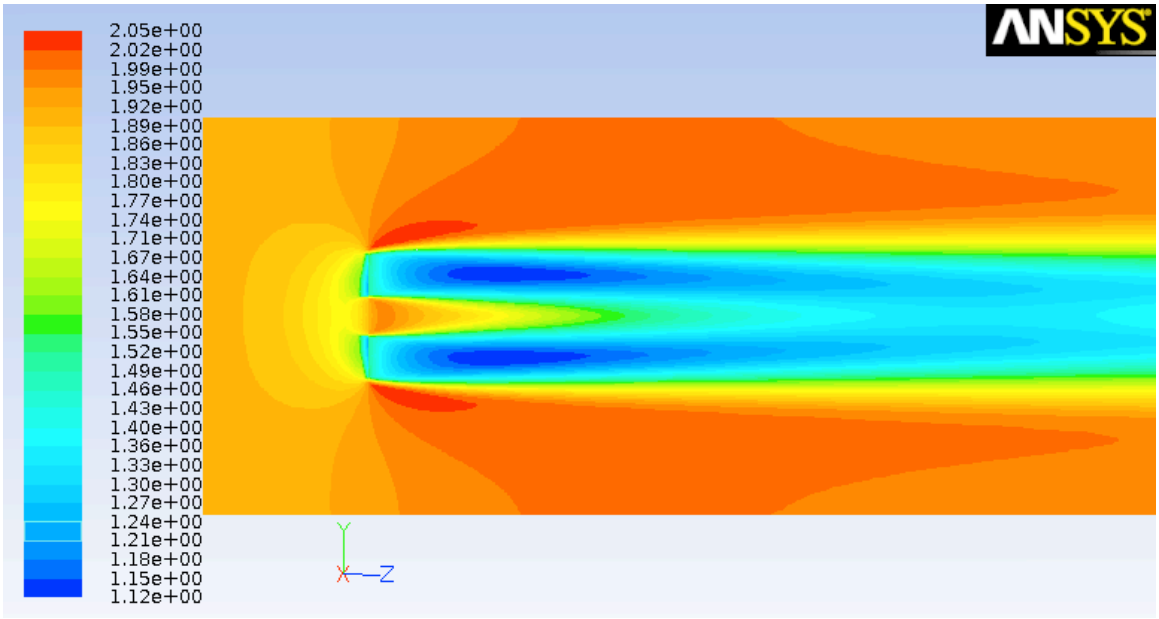

Figure n°27: Velocity magnitude contours for an efficiency of 20%

III.3) Comparison SRF/VBM

III.3.1) Power extracted

Two comparisons were made, using both turbulence models previously described: Spalart Allmaras and K-ω (with the corresponding VBM table of lift and drag coefficients as a function of angle of attack). The first one was computed with the density of fresh water, and the second one with values for seawater. Two different values of tip effect (as defined in …) have been studied for the VBM simulation: 98% and 96%.
To specify the turbulence, the turbulence intensity is still 5%, and the length scale is 1m. The free-stream velocity is 1.9m.s^{-1} and the rotor speed is 11.5rpm.
As a consequence, the tip speed ratio, defined as equation 53:

$$T.S.R. = \frac{r\omega}{U_\infty} \tag{53}$$

is equal to 6.3. This dimensionless number represents how fast the turbine is rotating with respect to the free-stream velocity.

The power calculated (and the efficiency corresponding, calculated thanks to equation (49)) are shown in table 7 .

Water	Power Spalart Allmaras (Efficiency)	Power SST K-ω (Efficiency)
SRF	351kW (η=35.41%)	495kW (η=49.94%)
VBM (TE=98%)	408kW (η=41.16%)	502kW (η=50.65%)
VBM (TE=96%)	356kW (η=35.92%)	446kW (η=45.00%)
Seawater	Power Spalart Allmaras (Efficiency)	Power SST K-ω (Efficiency)
SRF	359kW (η=35.27%)	511kW (η=48.64%)
VBM (TE=98%)	418kW (η=40.09%)	516kW (η=49.32%)
VBM (TE=96%)	365kW (η=35.86%)	458kW (η=45.00%)

Table n°7: Power and efficiency comparison between SRF and VBM simulations, for Spalart Allmaras and SST K-ω turbulence models

With regard to the efficiency, changing the fluid studied from water to seawater does not affect the simulations (the Reynolds number changes are negligible, of the order of 2%), and the power calculated increases normally because of the increase of the fluid density. The difference between the power calculated, taking the SRF simulation as a reference is presented in table 8.

Difference with respect to SRF simulation	Spalart Allmaras water	Spalart Allmaras seawater	SST K-ω seawater	SST K-ω water
VBM (TE=98%)	16.23%	16.43%	0.98%	1.41%
VBM (TE=96%)	1.42%	1.67%	10.37%	9.90%

Table n°8: Power gap between SRF and VBM simulations

We can see that the VBM simulation with a tip effect of 96% is matching the SRF simulation with the Spalart Allmaras turbulence model (difference of 1.42% and 1.67%), but it is not matching with SST K-ω (difference equal to 10.37% and 9.90%). Beside, it is the opposite with a tip effect of 98% (equivalent of 100% as explained in section III.2.1): matching with SST K-ω, but not with Spalart Allmaras.

Looking at the torque as a function of the position along the blade, and the fact that the torque for the last section of the blade is negative, it seems more accurate to have a tip effect 96%, which considers that the last section of the blade does not produce lift. Furthermore, previous studies on the NREL phase VI have been used to compare with the values obtained here. The results are listed in table 9.

Air	Power Spalart Allmaras	Power SST K-ω
SRF	5.244kW	5.975kW
VBM	5.414kW	4.734kW
Water	Power Spalart Allmaras	Power SST K-ω
SRF	106.54kW	125.28kW
VBM	99.185kW	97.258kW
Gap/SRF	Spalart Allmaras	SST K-ω
VBM (air)	3.24%	20.77%
VBM (water)	6.90%	22.37%

Table n°9: NREL phase VI data

These values confirm the idea that the Spalart Allmaras model is more adequate for the SRF simulation, and also the choice of a tip effect of 96% for the VBM simulation. To complete the study, velocity contours between the different simulations for the DOE reference model 1 have been compared.

III.3.2) Velocity contours

The study of the wake downstream the turbine is particularly important in the comparison of the two numerical models and in the study of the efficiency of an array of turbines.
From this perspective, the dimensionless freestream velocity magnitude is shown in figures 28 and 29, for the K-ω and the Spalart Allmaras turbulence models, respectively.
In each figure, SRF and VBM simulation velocity contours and selected velocity profiles are compared. The black lines represent the shape of the freestream velocity magnitude at selected distances downstream of the turbine: 1R, 3R, 5R, 7R, 9R and 11R, with R equal to one radius (10m)

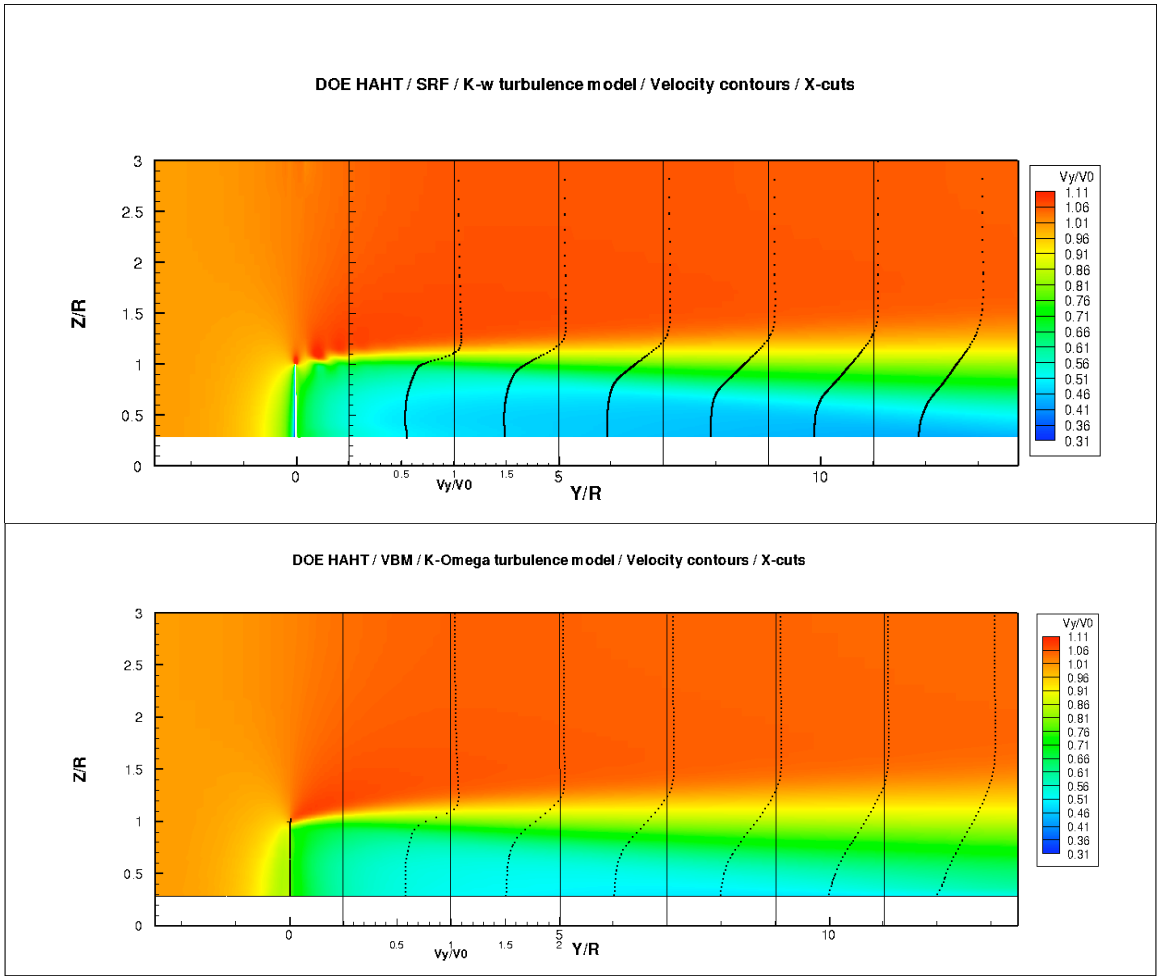

Figure n°28: Comparison of SRF and VBM contours of dimensionless free-stream velocity component for the K-ω turbulence model simulations at the center plane of the turbine rotor (x=0).

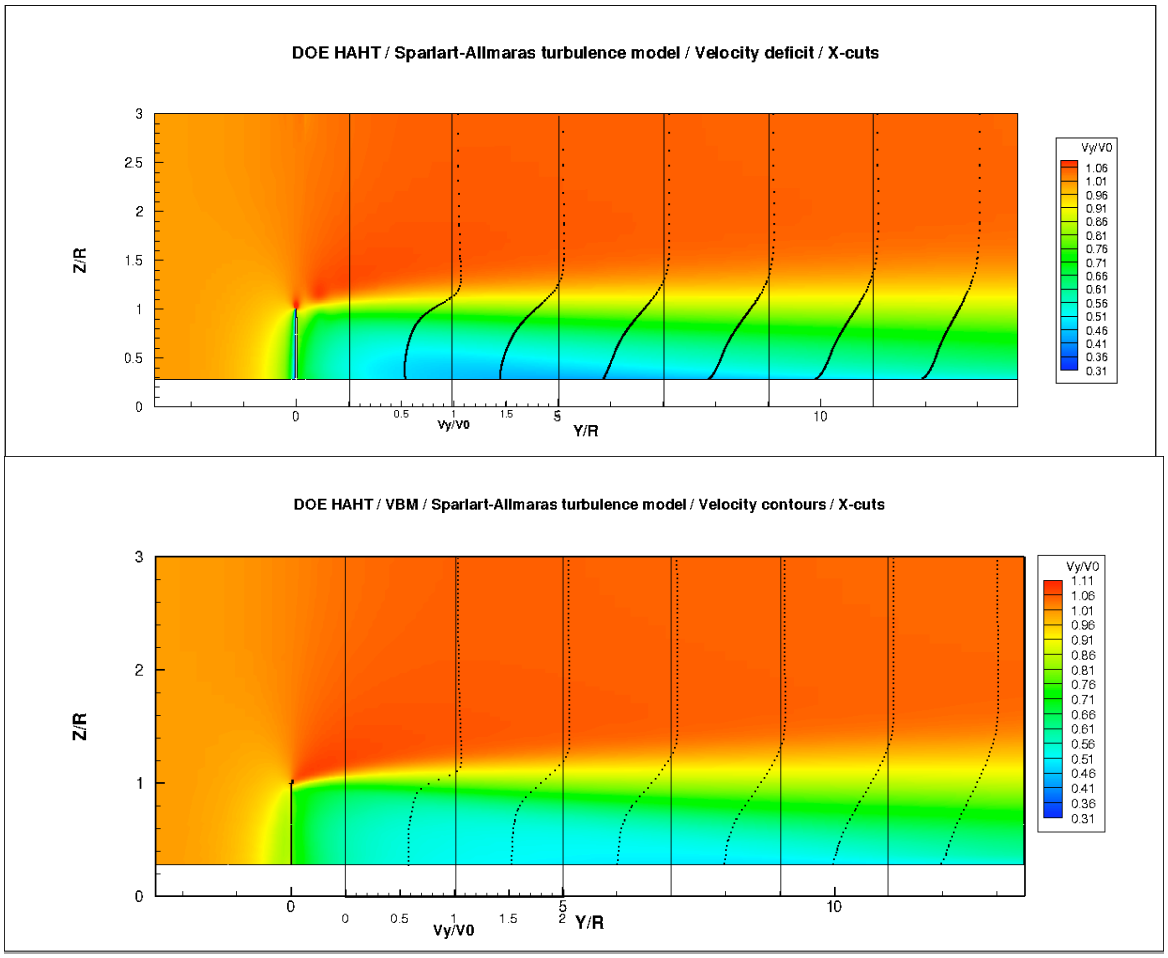

Figure n°29: Comparison of SRF and VBM contours of dimensionless free-stream velocity component for the Spalart Allmaras turbulence model simulations at the center plane of the turbine rotor (x=0).

The general shape of these contours is similar. There is a deceleration of the fluid upstream of the turbine. Downstream of the turbine, there is a large momentum deficit in the fluid. As the wake develops and entrains free stream fluid, this deficit tends to attenuate: in the far wake the velocity contours become flatter and flatter.

Close to the tip of the blade, we can see an acceleration of the flow, which is particularly marked by the presence of two vortices in the SRF simulations. This is the signature of the helical blade tip vortices seen in a cross plane. This vortex is closely associated with the loss of lift near the tip that has been discussed above in terms of the tip effect due to the 3D character of the flow in this region.

In the near wake, SRF and VBM seem to match for both turbulence models, but we can see a difference in the far wake for the two simulations that use the K-ω turbulence model. To have a better comparison of these models, only two velocity contours (one SRF and one VBM) are plotted at certain distances downstream the turbine: 1R, 5R, 9R and 11R (figure 30 and 31). In the abscissa we plot the dimensionless velocity, and for the ordinate we use the dimensionless position along the blade.

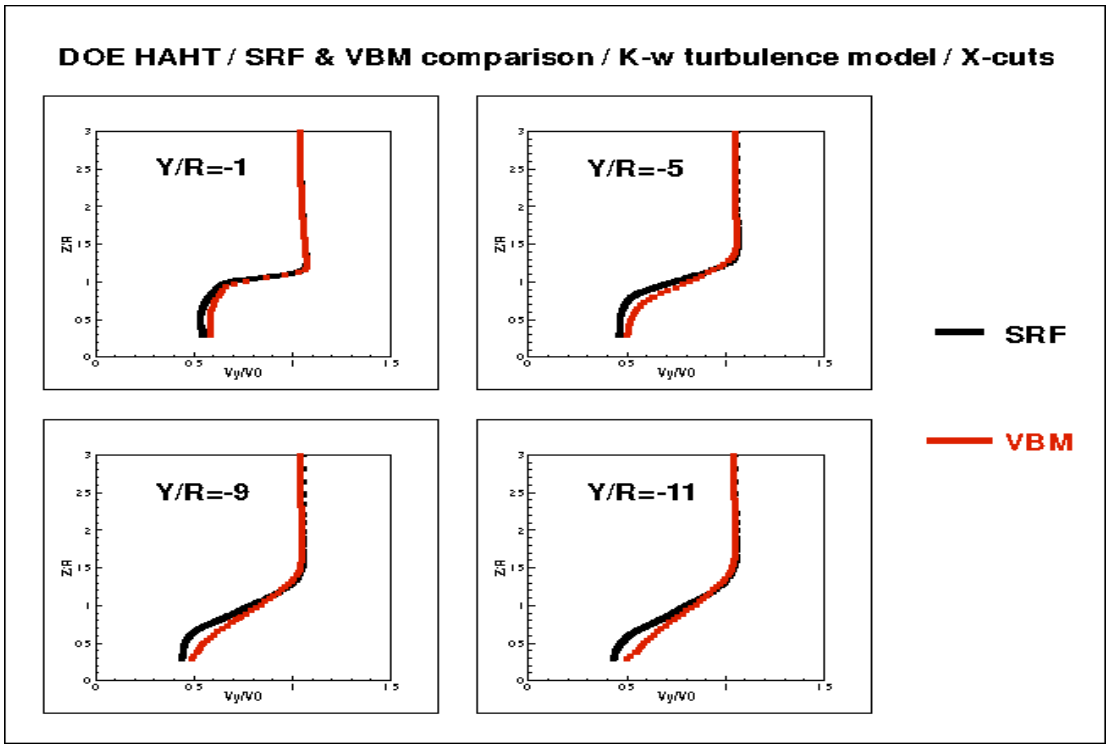

Figure n°30: Comparison of SRF and VBM velocity contours at four distances downstream the turbine for the K-ω turbulence model

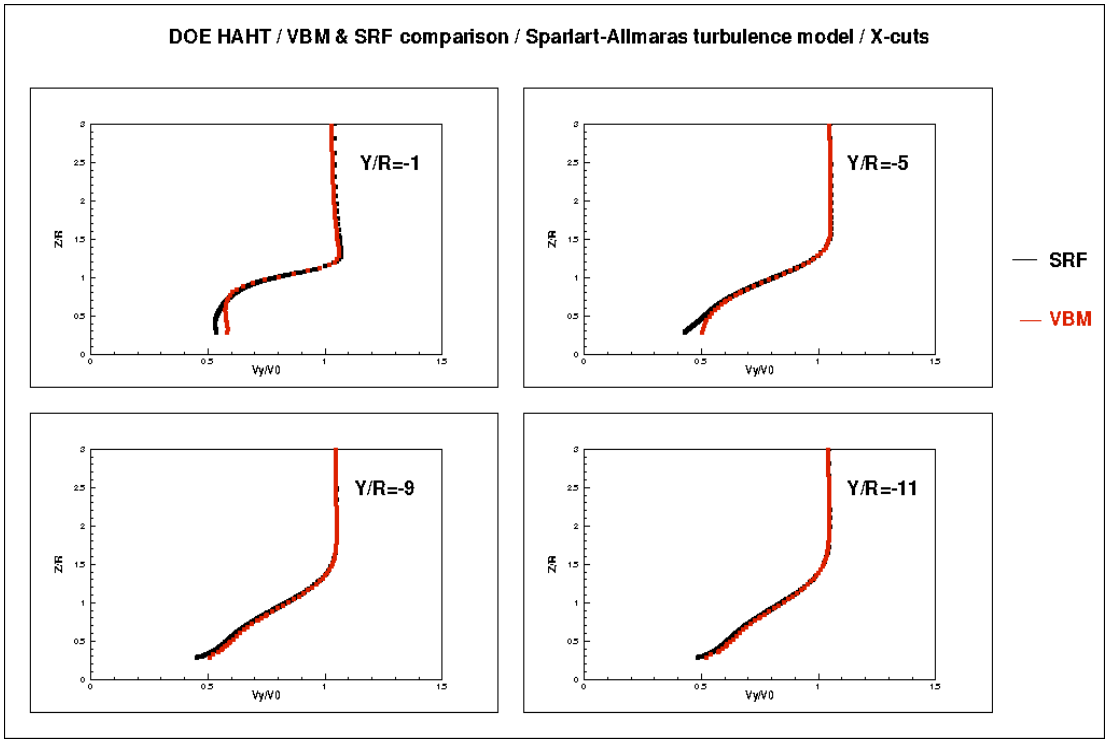

Figure n°31: Comparison of SRF and VBM velocity contours at four distances downstream the turbine for the Spalart Allmaras turbulence model

For the Spalart Allmaras model, the contours match well, especially after 5R downstream the turbine. The far wake is well represented. On the contrary, the velocity contours for SRF and VBM simulations using the K-ω model are not matching in the far wake, as can be seen in figure 30: we observe a significant difference in the shape close to the root of the blade.

These results confirm the idea that the Spalart Allmaras turbulence model is better adapted to study the flow on the turbine blade wall and, therefore, the performance of a hydrodynamic turbine. As a consequence, the lift and drag coefficients extracted from the Spalart Allmaras SRF simulation are used in the study of MHK turbine arrays, within the VBM framework, shown in the next chapter. The good match between SRF and VBM simulations support the use of the VBM methodology to study the flow in an array of MHK turbines, benefiting from the advantages of the VBM model (computational cost, lower requirements for mesh, …).

However, the K-ω model remains, in theory, better to study the wake of the flow downstream the turbine with VBM. Velocity contours downstream the turbine between the Spalart Allmaras VBM and K-ω VBM simulations have also been observed to be sensitive to the effect of changing the turbulence model in VBM (figure 32), allowing for the fact that K-ω under predicts the power extracted by the blade.

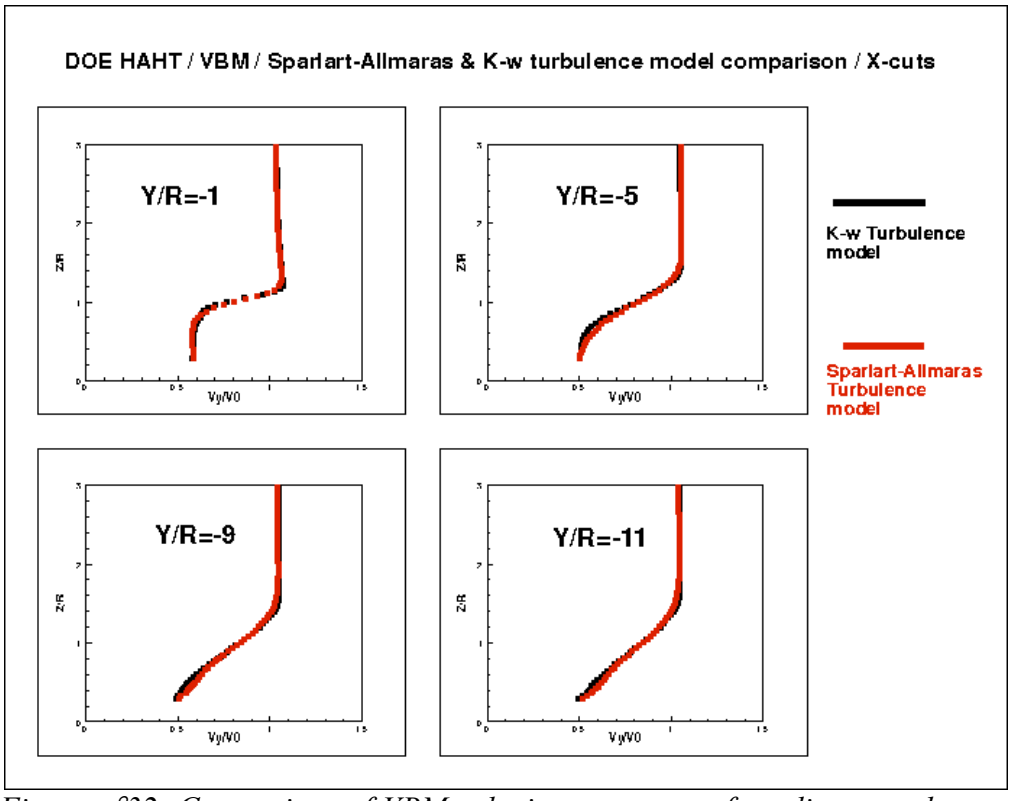

Figure n°32: Comparison of VBM velocity contours at four distances downstream the turbine for the Spalart Allmaras and the K-ω turbulence model

We can see that the velocity contours match well, so that the choice of the turbulence model does not affect significantly the wake of the flow downstream the turbine. As a consequence, the SST K-ω turbulence model will be used in the study of an array of turbines described in the following chapter, with lift and drag coefficients extracted from the SRF simulation with the Spalart-Allmaras turbulence model, which has been shown to predict the flow around the blade more accurately and therefore to produce lift and drag coefficients that match experimental results better.

IV) Array optimization

After studying one turbine, an array of turbine in a domain similar as what could be implemented is developed in this part. Based on the work of Mr. Cerisola Arthur, who has searched the optimal configurations in terms of extracted power (i.e. turbine position) for an array of 8 turbines with the geometry of NREL phase VI, two configurations (i.e. aligned and staggered) were created using the geometry of the DOE reference model 1. The goal here is two confirm or not the optimal configurations found previously with a new geometry, and a new domain.

IV.1) Description of the configurations

The two geometries were created with respect to [5]. In a row, the tip-to-tip distance is two radiuses.
For the first configuration (aligned), 3rd row turbines are aligned with upstream turbines of the 1st row. The turbines of the 2nd row have a lateral offset of 2 radiuses with the first row turbines. The downstream distance between the rows is 8 radiuses.
The 2nd configuration (staggered) has its 2nd row turbines staggered with a lateral offset of 1.5 radiuses from 1st row turbines, and 3rd row turbines also staggered with a lateral offset of 1.5 radiuses from 2nd row turbines (figure 33).

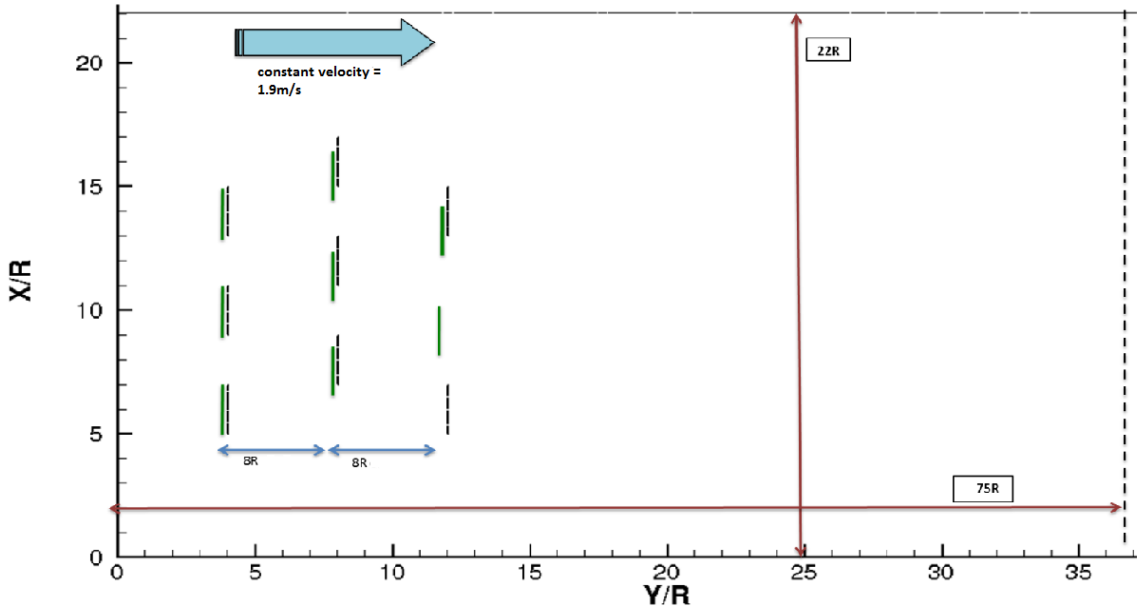

Figure n° 33: Aligned (black) and Staggered (green) geometries [5]

The channel has a rectangular cross section whose dimensions are 750m*220m*70m (75R*22R*7R). The last dimension is different from the 9R used with the NREL phase VI to have a realistic domain. Indeed, the total deep of the channel cannot be too increased and the radius of the DOE reference model 1 is bigger than NREL phase VI one (almost 2 times). As a consequence, the distance from the seabed will be proportionally smaller: the centers of turbine disks are located 20m from the seabed (2R, figure 34), compared to the 15m for NREL phase VI (2.7R(NREL phase VI)). The tip of the blade is located 10m from the seabed. The turbines disks are created with respect of the DOE reference model 1 geometry. The width of the channel avoids

any wall effects as acceleration of the flow and velocity variation on side turbines. Furthermore, walls boundary conditions will be set as velocity inlet to avoid these possible problems. The length is set of 75R to find a converged solution for the FLUENT simulation as regard to the wake behavior.

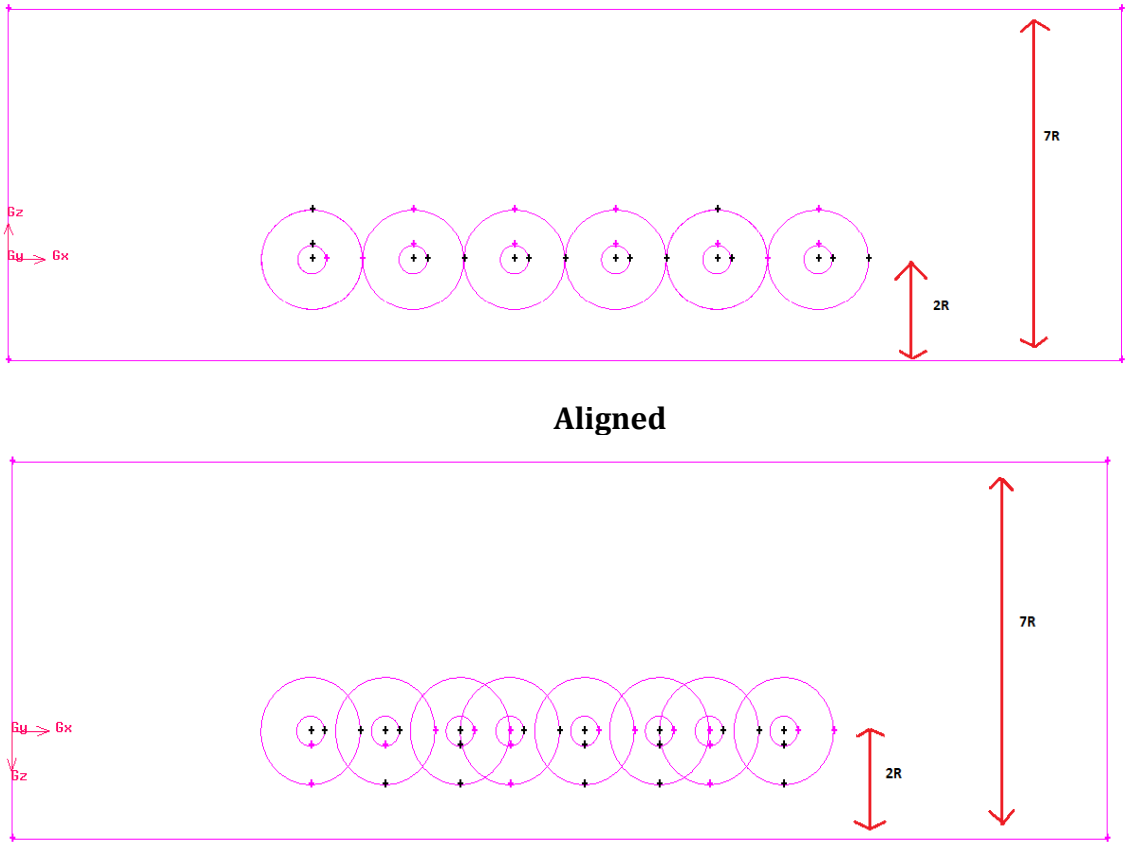

Figure n°34: Disposition of turbines in aligned and staggered configurations in Y-axis view

The mesh created are composed of 9 038 820 elements for the aligned configuration, and 8 892 856 elements for the staggered one. Two meshing methods were used: Hex/Wedge cooper, and Tet/Hybrid for the transition zones. The transition zones enable to change the lateral offset of a row of turbine, while keeping a good skewness of the mesh.

The settings of the simulations are listed table n°10

Material	Seawater
Turbulence model	SST K-ω
Turbulence intensity	5%
Turbulence length scale	1m
Free-stream velocity	1.9m/s
Rotor speed	11.5rpm
Pressure-velocity coupling scheme	SIMPLE
Discretization of gradient	Green-Gauss Node Based
Discretization of pressure	2nd order
Discretization of momentum	QUICK
Turbulent kinetic energy	1st order upwind
Specific dissipation rate	1st order upwind
Blade pitch	0deg

Table n°10: Operating conditions and solution method

IV.2) Results and discussion

The general shape of the velocity contours is similar to the one of NREL phase VI arrays (figure 35).

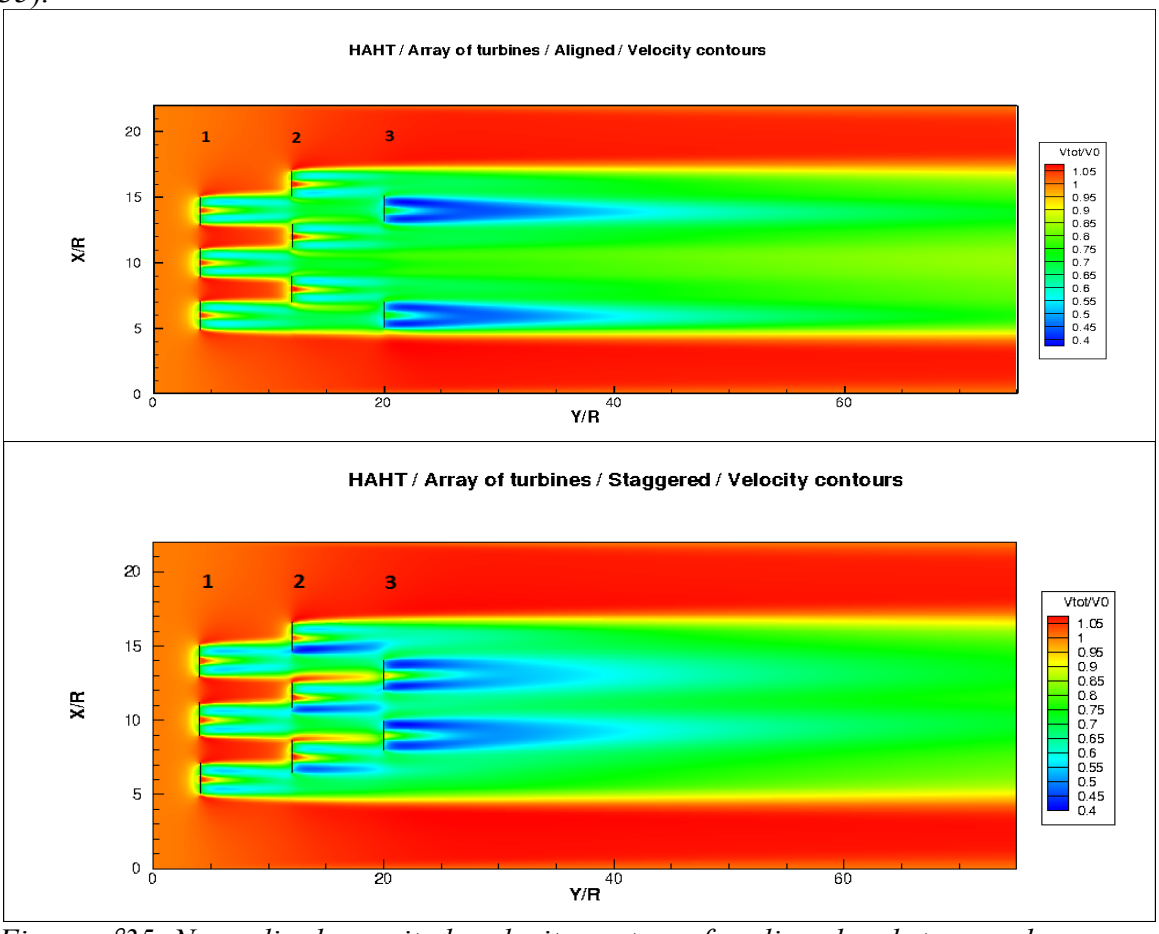

Figure n°35: Normalized magnitude velocity contours for aligned and staggered arrays

On both configurations, and at each row, we can see a velocity deficit just before the blade: the flow arriving on the turbines is affected by their rotation. Behind the blades, there is still a big velocity deficit as seen on a single turbine because of the extraction of power. In the wake of the blade, velocity increases progressively. The hub modeled by the porous zone defined with coefficients found in section III)2.2) also provides a big acceleration that decreases in the wake. Nonetheless, this effect does not have a big impact on the power extracted by downstream turbines, knowing the fact they are placed 8R downstream the previous row and so considered as far enough.
As observed with NREL phase VI turbine, the flow is accelerating around the tips of the blades due to the reduction of the cross-section area. Reference [5] proved it has no effect on downstream power extracted, but it also should be considered here.

After running first simulations, it has appeared that the angles of attack of the 2nd and 3rd rows from the staggered configuration and the 3rd row from the aligned configuration were not matching the good range defined in the table of lift and drag coefficients in function of angle of attack (appendix B). As a consequence, to complete these tables with a wider range of angles of attack, lift and drag coefficient values were interpolated for low angles of attack. The new good range of angles of attack for the table is now from 0.00° to 7.70°.
The power, minimum angle of attack and maximum angle of attack are listed table 11 for both configurations and each turbine.

Row.turbine (aligned)	Power (kW)	Minimum AOA	Maximum AOA
1.1	389	4.08°	7.12°
1.2	395	4.11°	7.11°
1.3	389	4.11°	7.11°
2.1	402	3.02°	7.27°
2.2	423	3.55°	7.40°
2.3	420	3.31°	7.40°
3.1	88	1.73°	5.73°
3.2	110	1.74°	5.36°
Row.turbine (staggered)	**Power (kW)**	**Minimum AOA**	**Maximum AOA**
1.1	388	4.10°	7.15°
1.2	395	4.12°	8.22°
1.3	388	4.10°	7.15°
2.1	324	1.27°	7.21°
2.2	369	1.60°	7.34°
2.3	390	1.97°	7.52°
3.1	227	1.56°	6.96°
3.2	199	1.65°	6.84°

Table n°11: Power extracted and range of angles of attack for turbines in an array

First, we can see that on the same row, each turbine does not have the same power. This can be explained by the position of the turbine and the way the flow attacking it behaves as regard to the effects of other turbines. On the first row, the turbine in the middle has a bigger power than the two side turbines due to a slight acceleration of the flow because of side turbines.
We can note the first row of both configurations have the same power extracted, which confirms the possibility to compare the two configurations, knowing they are experiencing the same operating conditions. Beside, these powers are bigger than the one found with the study of a single turbine. This can be explained by an acceleration of the flow due to the proximity of the seabed. Indeed, the need to have realistic distances made us moving the blade closer to the seabed as regard to the blade radius.

The second row of aligned configuration has a bigger power than the first row (+6.4%), even if their turbines have a lateral offset of two radiuses: an acceleration of the flow occurs and can be observed on velocity contours. The third row of this configuration has a very little power (loss of 74% of power compared to the 1st row): the wake of the flow has less energy to provide to the 3rd row (which has its turbines directly behind 1st row ones) due to the combined effect of 1st and 2nd row turbines, with major effect due to 1st row turbines, directly upstream.
For the staggered configuration, the two downstream rows extracts less power than the 1st row, which makes sense as regard to velocity contours. 2nd row have 7.4% less power and 3rd row 45% less than 1st row. This loss of 45% is far lower than the loss of 74% for the 3rd row of aligned configuration.

Average power for a row and an approximate local efficiency are listed table 12 . The local efficiency was calculated while evaluating the term V^3 in the total power available. This term was evaluating by taking the incoming velocity of the turbine 2R upstream the turbine, considering this distance is enough not to have an effect of the turbine downstream. Hence, the incoming velocity for the 3rd row of aligned configuration, 2nd row of staggered configuration and 3rd row of staggered configuration are evaluated respectively to 1.4m.s^{-1}, 1.8m.s^{-1} and 1.7m.s^{-1}, which represents tip speed ratios of 8.6, 6.7 and 7.1. We can see that even if the 3rd row of the aligned configuration has a very little power extracted, the local efficiency remains reasonable.

Row	Average power (aligned) (local efficiency)	Average power (staggered) (local efficiency)
1	390kW (38.32%)	390kW (38.32%)
2	415kW (40.78%)	361kW (41.73%)
3	99kW (24.31%)	213kW (29.23%)

Table n°12: average power and local efficiency for aligned and staggered arrays

IV.3) Comparison with NREL phase VI arrays

The difference of power on a fixed row between both configurations is first compares. For the DOE reference model 1, the 2nd row of aligned configuration extracts 13% more power than the 2nd row of staggered configuration. A based on [5] result, aligned configuration extracts 7% more than staggered one for 2nd row with NREL phase VI. Beside for the 3rd row, staggered configuration extracts 53% more power than aligned one with DOE reference model 1, and 27% with NREL phase VI. The evolution is similar, but figures are far bigger for the DOE reference model 1.

The total power extracted by the different configurations are shown table 13.

	Aligned DOE reference model 1	Staggered DOE reference model 1	Aligned NREL phase VI	Staggered NREL phase VI
Total power	2616kW	2680kW	776kW	782kW

Table n°13: Total power extracted by arrays of 8 turbines

With the NREL phase VI, we can extract 0.8% more power with 8 turbines in the staggered configuration than in aligned configuration. Similarly, with the DOE reference model 1, we can extract 2.4% more power in staggered configuration than in aligned one. This confirms the idea that the staggered configuration for an array of turbine is more efficient. Furthermore, even if the evolution of power is the same between the two blades studied here, it is important to note that figures found with the DOE reference model 1 are significantly bigger than with NREL phase VI. A first explanation could be the change of blade scale, but further investigations should be done to predict more generally the power extracted by an array of turbines.

CONCLUSION

The need for new renewable energies, and the cost and the difficulty of finding an adequate location for experimental research due to rare high speed current, has led the research on tidal turbines to rely heavily on computations. Based on the work of the mechanical engineering department of the University of Washington, Seattle (WA), especially the work of Mr. Arthur Cerisola and Mr. Teymour Javaherchi, a study of the DOE Reference Model 1 has been performed. Thanks to the methodology developed by the laboratory and the single rotating reference frame mesh done by Mr. Arthur Cerisola, a close study of the power and the velocity contours has been possible for a single turbine and for an array of turbines.

After analyzing the results of the SRF mesh previously done, it appeared that the root was responsible for a lot of uncertainty in the simulation. It has been decided to remove it; a new mesh has been designed on the base of the old one. As a result, the uncertainty was reduced and the computational time to converge was dramatically shortened. It was also possible to perform a study of the power differences without the root, composed mostly of elliptical blade sections. The results were acceptable (within 2%) because it was possible to match results done by another laboratory. But it appeared that considering the turbulence model, the power prediction, and therefore the efficiency, were very different. Knowing this, it has been decided to use the Spalart-Allmaras turbulence model, because it provides more rational results than the SST k-ω turbulence model.
After studying the SRF results, it has been decided to build the VBM simulations in the most accurate way possible; it was then possible to obtain results for large arrays in a reasonable computational time. After building an accurate lift-and-drag-coefficient-as-a-function-of-angle-of-attack look up table based on the SRF results, VBM matched the SRF results better with the Spalart-Allmaras turbulence model than with the SST k-ω. But the comparison of the VBM for the two turbulence model reveals that they provide similar velocity profiles in the wake. It has been decided that for the array of turbine the lift and drag coefficients table for each turbine will be based of the Spalart-Allmaras turbulence model. The simulations will then be run with the SST k-ω, because it is known to be more precise in the wake. The wake is indeed a high point of interest for an array of turbines. In parallel, the study of the ADM to model the hub as a porous zone has been performed.
Finally the study of an array of turbine based on the combination of the VBM and the ADM revealed that the DOE Reference Model 1 turbine set in a optimize configuration had a better efficiency than the NREL phase VI, for the same configuration. The preferred configuration is based on staggered rows, with a lateral offset of 1.5 radiuses between upstream and downstream turbines.

There is still a lot to learn on this technology, especially on arrays configurations that can change the efficiency, and where sedimentation may play an important role. Sedimentation changes the shape of the seabed and as a result the flow. The interaction with the free surface could also be interesting to study in order to measure the environmental effects of the turbine, for example on shipping. Finally a similar study as the one described here could be done for the same rotor design but at a different pitch. It is very likely that if an industrial model of the turbine were produced, it would be controlled with variable pitch in order to maintain constant the rotating speed of the blade.

Appendix A:

Blade geometry

	Radius (m)	**Pre-Twist** (deg)	**Chord** (m)	**Thickness** (m)	**Profile** (-)
Blade 0	1.75	12.86	1.118	0.703	naca 60629
Blade 1	2.05	12.86	1.386	0.615	naca 60444
Blade 2	2.35	12.86	1.61	0.53	naca 60329
Blade 3	2.65	12.86	1.704	0.47	naca 60276
Blade 4	2.95	11.54	1.662	0.43	naca 60259
Blade 5	3.25	10.44	1.619	0.4	naca 60247
Blade 6	3.55	9.5	1.577	0.378	naca 60240
Blade 7	3.85	8.71	1.534	0.368	naca 60240
Blade 8	4.15	8.02	1.492	0.358	naca 60240
Blade 9	4.45	7.43	1.45	0.348	naca 60240
Blade 10	4.75	6.91	1.407	0.338	naca 60240
Blade 11	5.05	6.45	1.365	0.328	naca 60240
Blade 12	5.35	6.04	1.322	0.317	naca 60240
Blade 13	5.65	5.68	1.279	0.307	naca 60240
Blade 14	5.95	5.35	1.235	0.296	naca 60240
Blade 15	6.25	5.05	1.192	0.286	naca 60240
Blade 16	6.55	4.77	1.148	0.276	naca 60240
Blade 17	6.85	4.51	1.103	0.265	naca 60240
Blade 18	7.15	4.26	1.058	0.254	naca 60240
Blade 19	7.45	4.03	1.012	0.243	naca 60240
Blade 20	7.75	3.8	0.966	0.232	naca 60240
Blade 21	8.05	3.57	0.92	0.221	naca 60240
Blade 22	8.35	3.35	0.872	0.209	naca 60240
Blade 23	8.65	3.13	0.824	0.198	naca 60240
Blade 24	8.95	2.9	0.776	0.186	naca 60240
Blade 25	9.25	2.67	0.726	0.174	naca 60240
Blade 26	9.55	2.43	0.676	0.162	naca 60240
Blade 27	9.85	2.18	0.626	0.15	naca 60240

Total radius: R=10m

Appendix B:

Lift and drag coefficients table

In red are comments about the structure of the table.

60240sa table name	7.70 1.28	4.07 0.04228
2 number of data	8.08 0.96	4.12 0.04118
cl 1st data: lift coefficient	8.74 0.91	4.20 0.04008
2000000 Reynolds number	10.34 0.86	4.30 0.03903
0.036 Mach number	13.11 0.74	4.41 0.03844
48 Number of lift coefficient	15.86 0.39	4.54 0.03770
-180.00 0.73 AOA Cl	16.00 0.39	4.70 0.03705
-150.00 0.73	18.00 0.39	4.87 0.03634
-120.00 0.73	20.00 0.39	5.06 0.03579
-80.00 0.73	30.00 0.39	5.28 0.03510
-40.00 0.73	40.00 0.39	5.52 0.03451
-30.00 0.73	60.00 0.39	5.79 0.03365
-20.00 0.73	80.00 0.39	6.08 0.03295
-10.00 0.73	120.00 0.39	6.42 0.03261
-6.00 0.73	160.00 0.39	6.79 0.03234
-4.00 0.73	180.00 0.39	7.21 0.03336
-2.00 0.73	cd 2nddata: drag coefficient	7.70 0.03482
0.00 0.73	2000000 Reynolds number	8.08 0.04237
2.00 0.73	0.036 Mach number	10.34 0.04982
3.00 0.73	46 Number of drag coefficient	13.11 0.16831
4.00 0.73	-180.00 0.04530 AOA Cd	15.86 0.44417
4.02 0.75	-160.00 0.04530	20.00 0.44417
4.07 0.77	-120.00 0.04530	30.00 0.44417
4.12 0.79	-80.00 0.04530	40.00 0.44417
4.20 0.80	-40.00 0.04530	80.00 0.44417
4.30 0.82	-30.00 0.04530	120.00
4.41 0.84	-20.00 0.04530	0.44417
4.54 0.85	-15.00 0.04530	160.00
4.70 0.87	-10.00 0.04530	0.44417
4.87 0.90	-6.00 0.04530	180.00
5.06 0.92	-4.00 0.04530	0.44417
5.28 0.95	-2.00 0.04530	
5.52 0.98	0.00 0.04530	
5.79 1.01	1.00 0.04530	
6.08 1.05	2.00 0.04530	
6.42 1.10	3.00 0.04530	
6.79 1.15	4.00 0.04530	
7.21 1.21	4.02 0.04359	

AOA: angle of attack

References

[1] Amir Teymour Javaherchi Mozafari. *Numerical Modeling of Tidal Turbines: Methodology Development and Potential Physical Environmental Effects.* Master thesis, November 2010.

[2] Sylvain Antheaume. *Modeling a Wind Turbine, Comparison of the SRF and VBM Models*. August 18, 2009.

[3] A. Gosset and G. Flouriot. *Optimization of Power Extraction in an Array of Marine Hydrokinetic Turbines.* Projet de Fin d'Etude, November 2010.

[4] F. Riesemann and M. Bewert. *Array Optimization of Marine Hydrokinetic Turbine.* Projet de Fin d'Etude, November 2011.

[5] A. Cerisola. *Numerical Analysis of Tidal Turbines Using Virtual Blade Model and Single Rotating Reference Frame.* Master thesis, August 2012.

[6] Kristen M. Thyng and James J. Riley. *Site Modeling for Tidal Turbines*. "2nd Annual OSU-UW Northwest National Marine Renewable Energy Center Conference", University of Washington, May 5, 2011.

[7] Pijush K. Kundu and Ira M. Cohen. *Fluid Mechanics, fourth edition.* USA: Elsevier, 2008. 880p. ISBN 978-0-12-373735-9.

[8] Stephen B. Pope. *Turbulent Flows.* New-York: Cambridge University Press, 2000. 776p. ISBN 978-0-521-59886-6.

[9] T.Burton, D.Sharpe, N.Jenkins and E.Bossanyi. *Wind Energy Handbook.* John Wiley & Sons, 2001. 642p. ISBN 978-0-471-48997-9.

[10] Juan Mendez and David Greiner. *Wind Blade Chord and Twist Angle Optimization by Using Genetic Algorithms.* "Proceedings of the Fifth International Conference on Engineering Computational Technology", Civil-Comp Press, Stirlingshire, UK, Paper 59, 2006.

[11] Michael J. Lawson, Ye Li and Danny C. Sale. *Development and Verification of a Computational Fluid Dynamics Model of a Horizontal-axis Current Turbine.* "Proceedings of the 30th international conference on ocean, offshore and arctic engineering", June 19-24 2011, Rotterdam, The Netherlands.

[12] Rahul Kumar. *Tutorial: Virtual Blade Model.* ANSYS FLUENT, 2007.

[13] ANSYS FLUENT 12.0, User's Guide. *Chapter 7, section 7.3.2, Using flow boundary conditions.* ANSYS FLUENT, 2009.